RESEARCH ARTICLE

Check for updates

Synthesis of Ananikov-type N-heterocyclic carbene golden synthons as ferroptosis inducing anticancer agents

Tommaso Lorenzon, [ID] †[a] Zisis Papadopoulos, [ID] †[b] Alessandro Rubbi, [ID] [a] Nicola Demitri, [ID] [c] Laura Orian, [ID] [a] Nicolás Montesdeoca, [ID] [b] Johannes Karges [ID] *[b] and Thomas Scattolin [ID] *[a]

The rational development of metal-based anticancer agents increasingly relies on precise ligand design and mechanistic understanding. Herein, we report the design, synthesis, and comprehensive evaluation of a new family of backbone-functionalized N-heterocyclic carbene (NHC) gold(I) complexes, enabled by a recent one-pot strategy for the preparation of heteroatom-decorated azolium salts. Using this approach, a library of 21 entirely novel Au(I)−NHC complexes was prepared, encompassing chloride, thiolate, aryl, and selenolate derivatives, representing the first systematic investigation of backbone-functionalized NHC ligands in gold-based medicinal chemistry. Efficient access to [Au(NHC)Cl] precursors was achieved *via* a weak-base metallation protocol, followed by mild, operationally simple, and environmentally benign transformations to structurally diverse Au(I) species. Multinuclear NMR spectroscopy and single-crystal X-ray diffraction confirmed the nature and stereoelectronic features of all complexes, while DFT calculations elucidated key mechanistic pathways, including gold−aryl formation and selenium-insertion reaction, highlighting the electronic influence of NHC backbone functionalization. Biological evaluation revealed pronounced anticancer activity for selected complexes, with compound **4b** exhibiting cytotoxicity exceeding that of cisplatin in several human cancer cell lines. Complementary fluorescence-based assays and confocal microscopy directly linked this activity to hallmark features of ferroptosis, including ROS generation, glutathione depletion, lipid peroxidation, and intracellular Fe^{2+} accumulation. Collectively, this work establishes backbone-functionalized Au(I)−NHC complexes as a new and versatile platform for ferroptosis-inducing metallodrugs, integrating synthetic innovation, mechanistic insight, and biological precision.

Introduction

The design of metal-based anticancer agents has evolved from empirical screening towards a rational, mechanism-driven approach grounded in coordination chemistry and molecular recognition. In this context, the choice and fine-tuning of the ligand framework have become central to controlling the stability, reactivity, and biological behavior of the final complex.[1,2] Among the many ligand families explored over the past two decades, N-heterocyclic carbenes (NHCs) have emerged as

uniquely powerful tools for constructing metal-based drugs with programmable properties.[3,4] Their remarkable σ-donor capacity, limited π-acceptor character, and strong resistance to oxidation impart outstanding stability to metal–NHC bonds, enabling the design of robust and modular complexes that remain intact under physiological conditions.

Initially developed as phosphine analogues, NHC ligands have since evolved into a cornerstone of organometallic medicinal chemistry, largely because of their ability to balance structural stability with tunable reactivity.[5] Subtle modifications to the carbene ring or to the substituents on the nitrogen atoms can dramatically alter both the electronic density at the metal center and the overall molecular topology, thus allowing precise control over key biological parameters such as lipophilicity, charge distribution, redox potential, and cellular uptake.[3–5] This intrinsic tunability distinguishes NHCs from other donor ligands and has made them indispensable in the quest for next generation metallodrugs.

[a]Dipartimento di Scienze Chimiche, Università degli Studi di Padova, via Marzolo 1, Padova, 35131 Italy. E-mail: thomas.scattolin@unipd.it
[b]Faculty of Chemistry and Biochemistry, Ruhr-University Bochum, Universitätsstrasse 150, 44780 Bochum, Germany. E-mail: johannes.karges@ruhr-uni-bochum.de
[c]Elettra – Sincrotrone Trieste, S.S. 14 Km 163.5 in Area Science Park, 34149 Basovizza, Italy
†These authors contributed equally to this work.

For bioinorganic applications, imidazol-2-ylidene derivatives bearing bulky *N*-substituents are typically favored. Their steric protection shields the metal center from undesired ligand exchange and prevents decomposition in aqueous media. However, these sterically encumbered ligands are chemically inert and devoid of functional groups capable of establishing secondary interactions with biological macromolecules, which are often essential for selectivity and efficient cellular targeting. To partially address this limitation, synthetic chemists have often modified one of the *N*-substituents with an alkyl chain containing a functional moiety (*e.g.*, thioether, sulfoxide, phosphonium).[6,7] This approach indeed introduces sites for secondary binding or hydrogen bonding but simultaneously compromises the kinetic inertness of the complex by reducing steric protection.

A conceptually superior yet synthetically challenging alternative involves decorating the NHC backbone (C4–C5 positions) with heteroatoms or functional groups, while maintaining bulky substituents on both nitrogen atoms. This design strategy preserves kinetic inertness while enabling new chemical interactions through the backbone substituents, which can act as hydrogen-bond donors/acceptors, redox-active centers, or coordination sites for secondary metal ions. Backbone functionalization also opens the door to multimetallic architectures and to conjugation with biologically relevant molecules such as steroids, carbohydrates, peptides, or antibodies —key features for the next generation of targeted metallodrugs. Despite these advantages, backbone-functionalized NHCs have historically remained scarce, mainly because their synthesis required long, multi-step procedures and harsh conditions incompatible with sensitive functional groups.[8,9]

A decisive breakthrough came in 2022, when the Ananikov group reported an innovative one-pot nucleophilic addition/ cyclization strategy that enables the preparation of heteroatom-functionalized imidazol(in)ium salts under exceptionally mild conditions.[10] This methodology tolerates a wide variety of nucleophiles and substituents, generating azolium salts with oxygen, sulfur, nitrogen, or halogen functionalities embedded directly in the carbene backbone. The simplicity, scope, and operational greenness of this reaction make it ideally suited for producing libraries of tailor-made NHC precursors previously inaccessible by conventional routes.

The present work exploits this synthetic advance to create a series of gold(I)–NHC complexes bearing heteroatom-functionalized backbones, specifically designed for biological applications. All the compounds reported herein are completely novel, representing the first exploration of such ligands in gold-based anticancer chemistry.

The use of gold(I) as the metal center is motivated by its unique redox and coordination chemistry. Gold(I) exhibits strong affinity for soft donor atoms such as sulfur and selenium, forming highly stable linear complexes that are resistant to hydrolysis yet reactive toward biomolecular thiols.[11] Through these interactions, gold(I) species can disrupt the redox balance of cancer cells by inhibiting thioredoxin reductase (TrxR) and depleting intracellular glutathione (GSH),

two key components of the antioxidant defense network.[12,13] This redox interference leads to reactive oxygen species (ROS) accumulation, oxidative stress, and ultimately cell death.

Within this mechanistic framework, gold(I) complexes bearing NHC ligands have emerged as particularly promising scaffolds. The interest in Au(I)–NHC compounds as anticancer agents dates back more than a decade, with early seminal work demonstrating that lipophilic Au(I)–NHC architectures exhibit marked cytotoxicity and mitochondrial perturbation, thereby establishing the therapeutic relevance of this ligand class.[14] Subsequent studies by multiple groups expanded this concept and revealed clear structure–activity relationships governing their biological response.[15–18] In general, increased steric bulk and lipophilicity of the NHC substituents enhance cellular uptake, while backbone functionalization can also significantly modulate cytotoxic activity.

In our previous 2025 study, we performed a systematic investigation of the biological activity and reactivity of several classes of gold(I)–NHC fragments, identifying three particularly promising categories: Au–Cl, Au–aryl, and Au–thiolate complexes.[19] These species represent the most synthetically versatile and biologically relevant subfamilies within gold(I)–NHC chemistry. Notably, the Au–Cl fragment serves as a central synthetic synthon, often used as a precursor for nucleophilic substitution or transmetallation reactions that yield the Au–thiolate and Au–aryl derivatives.[20]

As emphasized in a recent review,[20] such structural interrelationships among gold(I) complexes establish a synthetic continuum, where specific fragments act as versatile building blocks for the construction of new generations of organogold compounds. Understanding this network of interconversions is crucial for controlling reactivity, tuning biological performance, and designing efficient synthetic routes.

Our 2025 investigation provided not only a framework for interpreting these chemical relationships but also a pivotal biological discovery: the identification of [IPrAu(SPh)] as the first mononuclear gold(I)–NHC complex capable of inducing ferroptosis.[19] This finding revealed an unexpected dimension of gold–NHC reactivity. Until then, Au–NHC complexes had been primarily associated with apoptotic or mitochondrial pathways of cell death, typically arising from oxidative stress or enzyme inhibition.[12–18] The demonstration that [IPrAu(SPh)] could trigger ferroptosis—a completely distinct, iron-dependent form of regulated cell death[21]—established a new paradigm in gold-based medicinal chemistry. Ferroptosis is characterized by glutathione depletion, inactivation of lipid repair systems, uncontrolled peroxidation of polyunsaturated phospholipids, and profound membrane damage, ultimately leading to cell demise.[21] Unlike apoptosis, it does not involve caspase activation or classical morphological hallmarks, but instead reflects a metabolic and redox-driven collapse of lipid homeostasis.

From a therapeutic standpoint, ferroptosis has emerged as a particularly attractive mechanism for metallodrug development in oncology. Many aggressive or drug-resistant tumors display vulnerabilities in iron metabolism, redox regulation,

and lipid handling that can be selectively exploited by ferroptotic stimuli.[21b] Inducing ferroptosis therefore offers opportunities to overcome apoptosis resistance, target metabolically rewired cancer cells, and synergize with established treatments.

In this context, the observation that a structurally simple Au(I)–NHC complex could act as a ferroptosis inducer significantly broadened the conceptual scope of gold-based therapeutics.

To date, no other gold(I)–NHC complexes have been shown to elicit ferroptotic mechanisms, highlighting both the novelty and the untapped potential of this chemical space.

Beyond NHC frameworks, only a few gold complexes have ever been reported to induce ferroptosis, emphasizing the rarity of this phenomenon across gold chemistry. The best-known example is Auranofin, a gold(I)–phosphine–thioglucose drug that can trigger ferroptosis alongside apoptosis through TrxR inhibition, ROS overproduction, and lipid peroxidation.[22] More complex architectures, such as NIR–AIE-based theranostic systems,[23] and particular gold nanoclusters,[24] have also been shown to modulate ferroptosis, albeit through diverse and often overlapping redox pathways involving GSH/GPX4 depletion and thiol exchange processes.

Altogether, these few precedents confirm that ferroptosis induction by gold compounds—whether NHC- or non-NHC-based—is an exceptional event that requires fine-tuning of the metal–ligand environment. Within this emerging context, [IPrAu(SPh)] remains the only mononuclear gold(I)–NHC complex unambiguously proven to activate ferroptosis, setting a mechanistic benchmark for the rational design of new ferroptosis-inducing metallodrugs.

The present study aims to expand this frontier by combining innovative ligand design with mechanistic and biological exploration. Building upon our previous findings, we now investigate not only the Au–Cl, Au–aryl, and Au–thiolate motifs but also the recently reported Au–selenolate complexes, a class introduced by Nolan and Ott that features selenium donors in place of sulfur.[25]

By integrating state-of-the-art synthetic innovation, mechanistic computation, and targeted biological evaluation, this study aims to establish a new generation of gold(I)–NHC complexes that merge backbone functionalization and biological precision. The inclusion of heteroatom-decorated NHC ligands and diverse Au(I) fragments offers an unprecedented opportunity to expand the chemical, structural, and mechanistic diversity of gold-based ferroptosis inducers.

Results and discussion

Synthesis and electronic properties of backbone functionalized NHC precursors

Our work began with the synthesis of backbone-functionalized azolium salts, following the procedure reported by Ananikov and co-workers in 2022.[10] In particular, with the aim of exploring both the influence of the N-substituents and the nature of
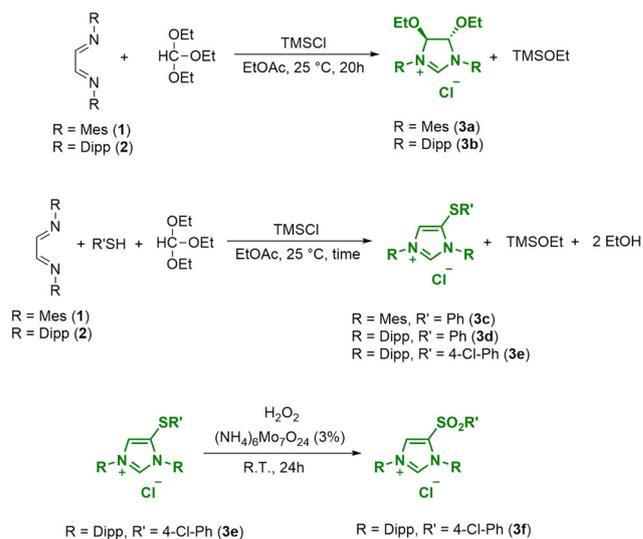
Scheme 1 Synthetic routes to backbone functionalized azolium salts **3a–f**.

the functional group installed on the backbone, we selected the azolium salts shown in Scheme 1. These compounds feature either the bulky and widely used 2,4,6-trimethylphenyl or 2,6-diisopropylphenyl substituents on the nitrogen atoms, combined with ether or thioether functionalities along the backbone. These groups can be conveniently introduced through a one-pot reaction starting from readily available N,N'-diaryl-1,4-diaza-1,3-butadiene precursors, which were prepared on a multigram scale from commercially available anilines and glyoxal.[26]

Specifically, azolium salts **3a–e** are obtained through a multicomponent nucleophilic addition–cyclization reaction between triethyl orthoformate and N,N'-diaryl-1,4-diaza-1,3-butadienes, in the presence of a nucleophile and a promoter such as trimethylchlorosilane (TMSCl) (Scheme 1).[10] In this process, the diazabutadiene provides the nucleophilic nitrogen atoms that react with the pre-carbene carbon of the orthoformate, while its electrophilic C2 and C3 carbons can form bonds with heteroatomic nucleophiles. Interestingly, when no external heteroatomic nucleophile is added, the orthoformate acts simultaneously as a C1 building block and as a source of ethoxy groups, whereas TMSCl promotes the transformation and provides chloride ions. Under these conditions, the reaction furnishes 4,5-diethoxy-imidazolinium salts, as in the case of compounds **3a–b** prepared in this work.

Although the reaction can also proceed in the presence of HCl or other acids (e.g., HBr, HI, HBF4), the best results are achieved using TMSCl as the promoter and ethyl acetate as the solvent, under aerobic and ambient conditions. When the same reaction is carried out in the presence of an efficient heteroatomic nucleophile such as thiophenol or 4-chlorothiophenol, the process leads to the formation of unsaturated azolium salts **3c–e**, each featuring a single thioether substituent in the backbone. The mechanistic details underlying this divergent

behavior (monosubstitution *vs.* disubstitution and formation of saturated *vs.* unsaturated azolium salts) have been thoroughly discussed by Ananikov and co-workers.

All azolium salts, whether containing ether or thioether functionalities, were isolated by simple filtration of the crude reaction mixture, owing to their poor solubility in ethyl acetate, and obtained in yields comparable to those reported in the literature.

To slightly expand the scope of backbone-functionalized carbene precursors available for subsequent metalation steps, we decided to oxidize the imidazolium salt **3e** to the corresponding sulfone derivative **3f**, following a recent procedure (Scheme 1).[27] In this transformation, hydrogen peroxide is employed as the oxidant in the presence of a molybdenum catalyst. We reasoned that the introduction of a sulfone group —owing to its strong electron-withdrawing nature—could significantly decrease the donor ability of the corresponding carbene, while at the same time offering potential for hydrogen-bond interactions with biological targets.

Similarly to the other derivatives, compound **3f** was obtained simply by filtration of the solid formed in the reaction mixture, followed by washing with cold water, affording the desired product in yields consistent with those reported in the recent literature.

To confirm the successful formation of all azolium salts, we recorded their ^{1}H NMR spectra, which are fully consistent with those previously reported in the literature.

Beyond verifying the reaction outcomes, the ^{1}H NMR data also provide valuable insight into the electronic characteristics of these compounds, which is particularly relevant to their use as carbene ligand precursors.

Indeed, according to a method recently developed by Szostak and Nolan, the pure σ-donor strength of a carbene ligand can be correlated with the ^1J(C–H) coupling constant between the NCHN carbon and its proton in the corresponding azolium salt.[28] Practically, this coupling constant can be determined from the satellite peaks of the NCHN proton, which appears at relatively high chemical shifts due to its pronounced acidity.

In the Szostak–Nolan scale, a greater ^1J(C–H) value indicates a weaker σ-donor character of the carbene derived from the respective azolium salt.

Plotting the ^1J(C–H) values determined from the ^{1}H NMR spectra (see Fig. 1)—including those of non-functionalized reference salts (IPr·HCl and SIPr·HCl)—allows several clear trends to emerge: (i) carbenes featuring two ethoxy groups on the backbone are slightly weaker σ-donors, yet of comparable magnitude, compared to their non-functionalized saturated analogues (*e.g.*, SIPr); (ii) carbenes bearing a single thioether substituent in the backbone show similarly modest decreases in σ-donor ability compared with the corresponding non-functionalized unsaturated analogues; (iii) oxidation of the thioether moiety to a sulfone results in a pronounced reduction of σ-donor strength in the derived carbene; (iv) a slight increase in σ-donation is observed upon replacing 2,4,6-trimethylphenyl with 2,6-diisopropylphenyl substituents on the nitrogen atoms, consistent with hyperconjugative effects.
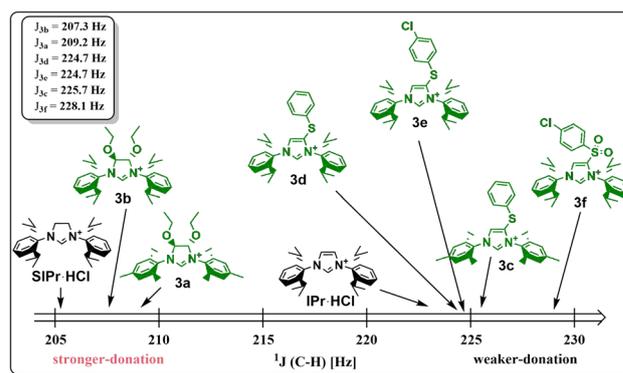

Fig. 1 ^1J(C–H) coupling constants of backbone functionalized and non-functionalized azolium salts (in DMO-d$_6$).

The σ-donor character of the N-heterocyclic carbenes was further rationalized by DFT calculations, in the attempt of providing insight into their electronic influence on the interaction with the gold(I) center. These computational analyses, reported in the SI (see ASA/EDA of [Au(NHC)Cl] complexes section), which seem to correlate with the experimental ^1J(C–H) coupling constants, elucidate how backbone functionalization modulates the σ-donor strength of NHCs, thereby providing a rationale for the NMR scale. However, further investigation is necessary for a quantitative explanation, which is out of the focus of this work.

Synthesis of gold(I)-chloride complexes bearing backbone functionalized NHCs

Once the backbone-functionalized azolium salts had been synthesized, we began exploring the gold chemistry of these proligands by preparing the corresponding [Au(NHC)Cl] complexes.

[Au(NHC)Cl] complexes are among the most studied gold(I) species, owing to their crucial role both in catalysis and medicinal chemistry. In catalysis, they serve as efficient precatalysts that, upon halide abstraction, generate the active cationic species [Au(NHC)]$^+$ used in a variety of transformations such as alkyne hydration, hydroamination, cycloisomerization, enyne cyclization, and nucleophilic additions to π-activated substrates.[29,30] In medicinal chemistry, these complexes display notable antitumor activity, largely attributed to the inhibition of thioredoxin reductase and disruption of redox homeostasis, which induces oxidative stress and apoptosis in cancer cells.[11–13] Moreover, [Au(NHC)Cl] complexes act as versatile synthons for the preparation of numerous gold derivatives,[20] some of which are presented in the following sections of this contribution.

Regarding their synthesis, [Au(NHC)Cl] species can be obtained through the "weak-base" route using mild bases such as K$_2$CO$_3$,[31,32] NaOAc,[33] or aqueous ammonia,[34] offering significant advantages over the classical free-carbene and silver-transmetallation methods.[5] In this approach, the metal-assisted deprotonation of the azolium salt occurs in the pres-

ence of a gold(ɪ) precursor (*e.g.*, [Au(DMS)Cl] (DMS = dimethyl-sulfide)), allowing immediate coordination of the carbene without isolation of a free NHC. This one-pot, mild, and air-tolerant procedure avoids the need for strong bases or silver reagents, thus reducing waste and simplifying purification.

In addition, the weak-base strategy generally provides higher isolated yields and enables straightforward scalability of the synthesis, including multigram-scale preparations or larger, while maintaining reproducibility. The operational simplicity of the protocol often results in minimal purification requirements, frequently involving only simple work-up procedures or, in some cases, no chromatographic purification at all.

Notably, a very recent mechanistic study reported by our team and the Nolan group have refined the mechanistic picture previously proposed for this transformation (Scheme 2B).[34a] The original mechanism invoked a concerted deprotonation–metallation process, in which the weak base, the azolium substrate, and the gold(ɪ) precursor would simultaneously participate in a single transition state, leading directly to [Au(NHC)Cl] with loss of chloride and without detectable intermediates.[35] Although consistent with the

experimental absence of free carbenes, this three-body concerted step was judged statistically improbable. The revised mechanism instead proceeds through two sequential steps: first, a slow deprotonation of the azolium salt by the weak base generates a transient carbene species, followed by rapid metallation through reaction with the $AuCl_2^-$ anion to afford the final complex.[34a] The free carbene thus formed exists only fleetingly, never accumulating to detectable concentrations, which reconciles both the experimental evidence and the kinetic plausibility of the process.

Armed with all this information, we successfully synthesized the gold(ɪ)–chloride complexes **4a–f** by direct reaction of the azolium salts **3a–f** with [Au(DMS)Cl] in the presence of potassium carbonate (3 equiv.) as a mild and inexpensive base (Scheme 2A). In all cases, the reaction proceeded to full conversion within 4 hours at 60 °C under aerobic conditions, using technical-grade acetone (green acetone) as solvent. The products were isolated simply by removing the solvent, adding a small aliquot of dichloromethane, filtering through a short pad of silica to remove inorganic salts, and evaporating the amount of dichloromethane. The resulting complexes were obtained as white solids in excellent purity and yields, typically around 90%, both on the milligram and gram scales, demonstrating the scalability and robustness of the process.

The ^1H NMR spectra show, besides the general shift of all signals compared to the starting azolium salts, the complete disappearance of the resonance associated with the co-ordinated dimethyl sulfide ligand of the gold precursor, as well as the absence of the characteristic azolium NCHN proton, clearly indicating successful carbene metallation at the gold(ɪ) center. In the ^{13}C NMR spectra, a new resonance appears in the range 177–198 ppm, depending on the saturation of the imidazole ring, which is diagnostic of a carbene carbon bound to gold(ɪ).

The solid-state structure of complexes **4a**, **4b**, **4d** and **4e** were resolved by X-ray single crystal diffraction and used to confirm the successful outcome of the reactions (Fig. 2). Single crystals were obtained by slow evaporation of diethyl ether into a chloroform solution of the complex at 4 °C.

The structural data confirm the expected atomic connectivity and reveal a Au–Cl bond length of *ca.* 2.27 Å, a carbene–Au bond length of *ca.* 1.97 Å, and a C–Au–Cl angle between 175° and 177°. The C–C bond length in the NHC backbone is approximately 1.53 Å for saturated systems and 1.34 Å for unsaturated ones, consistent with their respective hybridization patterns.

Synthesis of gold(ɪ)-aryl complexes bearing backbone functionalized NHCs

The second class of compounds investigated in this work comprises gold(ɪ)–aryl complexes, which represent a valuable family of gold(ɪ)–NHC synthons. These species are often invoked as key intermediates in gold-catalysed transformations and have recently gained attention due to their potential synthetic utility.[36] Historically, their preparation relied on the reaction between [Au(NHC)Cl] and aryl Grignard reagents, a
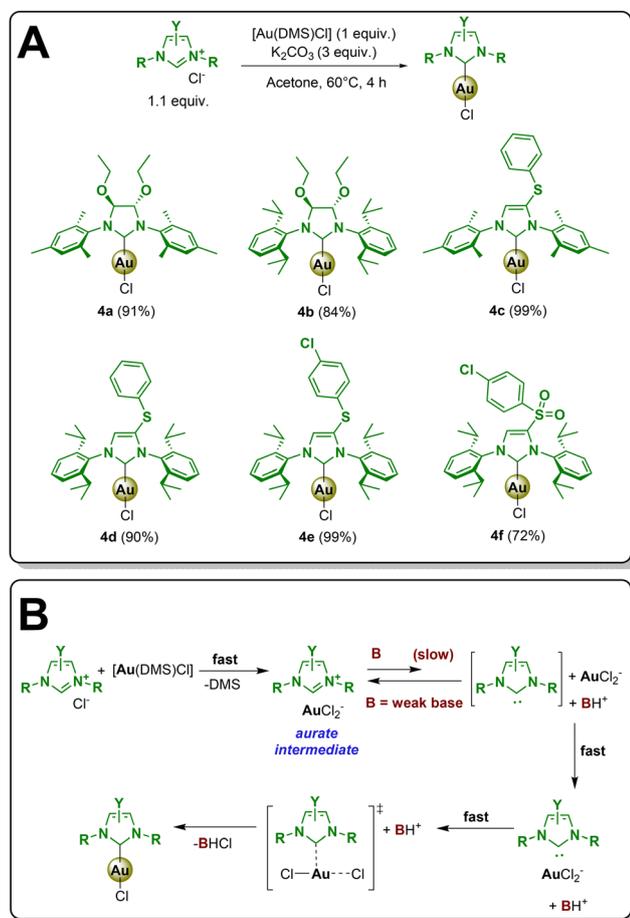
Scheme 2 Synthetic route to gold(ɪ)–chloride complexes (A) and proposed mechanism (B).
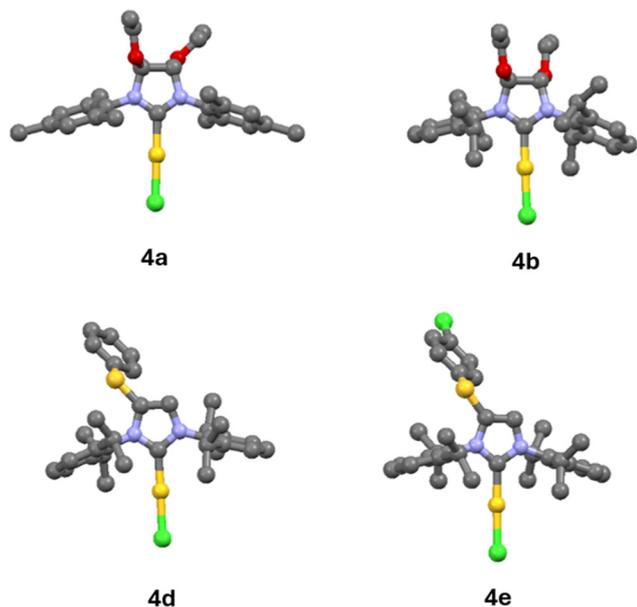
Fig. 2 X-ray molecular structures of complexes **4a**, **4b**, **4d** and **4e** are presented, with hydrogen atoms and solvent molecules omitted for clarity.

Scheme 3 Synthetic route to gold(ı)–aryl complexes.

procedure that suffers from the typical drawbacks of Grignard chemistry, including air sensitivity, poor functional group tolerance, and laborious purification steps.[37]

Modern synthetic methodologies have overcome these limitations through milder and more versatile transmetalation or decarboxylation routes. Among these, base-assisted transmetalation between aryl boronic acids (or esters) and NHC–Au (ı) precursors has become the method of choice. Initially reported by Gray and co-workers, this reaction involves the coupling of $[Au(L)X]$ (L = PR$_3$, NHC; X = Cl, Br) with aryl boronic acids in the presence of cesium carbonate, affording $[Au(NHC)(aryl)]$ complexes in good to excellent yields.[38] Subsequent refinements by Nolan and co-workers demonstrated that the hydroxo complex $[Au(IPr)(OH)]$ can react quantitatively with aryl boronic acids or trifluoroboronates at room temperature under exceptionally mild conditions.[39]

More recently, Nolan and colleagues developed an even simpler approach based on the reaction of $[Au(IPr)Cl]$ with a slight excess of an aryl boronic acid in the presence of a weak base such as K$_2$CO$_3$.[40,41] The method displays broad functional group compatibility—tolerating both electron-donating and electron-withdrawing substituents on the aryl moiety—and is applicable to a variety of NHC ligands. Importantly, this mild, weak-base protocol also enabled the development of an efficient continuous-flow process for the synthesis of NHC–Au (ı)–aryl complexes.[42,43]

Following the weak-base protocol, we successfully synthesized a selection of 8 novel gold(ı)–aryl complexes featuring backbone-functionalized NHC ligands (Scheme 3). The aryl fragments employed included both the unsubstituted phenyl group and derivatives bearing electron-withdrawing
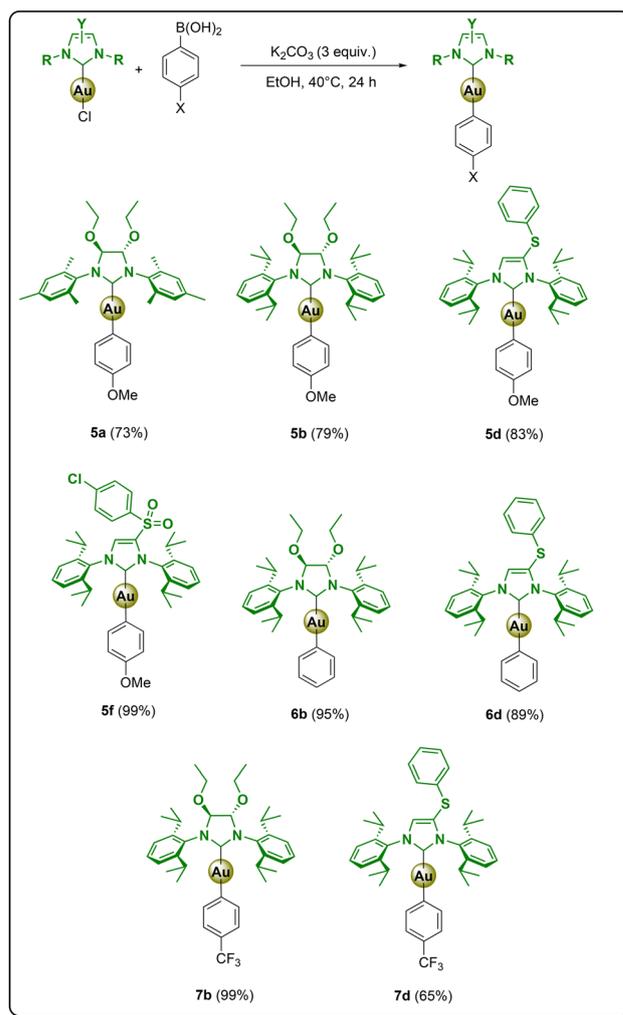
(4-trifluoromethylphenyl) or electron-donating (4-methoxyphenyl) substituents. This study was designed to explore whether variations in the NHC backbone and the aryl substituents could influence the antitumor activity of gold(ı)–aryl complexes.

All reactions were carried out at 40 °C under aerobic conditions in technical-grade ethanol, using gold(ı) chloride complexes as precursors, aryl boronic acids as aryl sources, and potassium carbonate as a weak and inexpensive base. After 4 hours, the solvent was removed under reduced pressure. Dichloromethane was then added, and the resulting mixture was filtered through a PTFE membrane to remove traces of gold nanoparticles and all inorganic salts. Precipitation from a dichloromethane/pentane mixture afforded the desired products as white solids in good isolated yields, ranging from 65% to 99%.

All compounds were comprehensively characterized by ^{1}H and ^{13}C NMR spectroscopy. In the ^{1}H NMR spectra, clear chemical shift differences were observed with respect to the parent gold(ı)–chloride complexes, along with the appearance

of new aromatic resonances attributable to the aryl fragment coordinated to the gold(I) center. These signals are found at distinct chemical shift values compared to those of the corresponding aryl boronic acids, confirming the successful formation of the Au–C(aryl) bond.

Similar observations were made in the ^{13}C NMR spectra, where the characteristic resonance of the carbene carbon remains detectable at high chemical shift values, together with new signals in the typical aromatic region corresponding to the gold–aryl moiety.

Further confirmation of the molecular structure was obtained for complex **5a**, whose solid-state structure was determined by single-crystal X-ray diffraction (Fig. 3). Suitable crystals were grown by slow diffusion of *n*-pentane into a chloroform solution of the compound at 4 °C. The crystallographic analysis revealed a nearly linear coordination geometry around the gold(I) center, with an Au–C(aryl) bond length of approximately 2.08 Å, a C–C bond length in the NHC backbone of about 1.53 Å, and a carbene–gold–aryl bond angle of *ca.* 177°. The Au–C(carbene) bond length was found to be approximately 2.06 Å.

Despite the synthetic relevance of this weak-base approach, its reaction mechanism remains unexplored.

To elucidate the mechanism of gold–aryl coupling, a study was conducted *in silico* using a simplified Au(I)–NHC chloride complex ([[(1,3-bis(2,6-dimethylphenyl)4,5-dimethoxyimidazol-2-ylidene)AuCl], **4**) and phenylboronic acid, at the COSMO-ZORA-PBE0/TZ2P-ae//ZORA-BLYP-D3(BJ)/TZ2P level of theory (for details, see SI).[44–49] Two plausible mechanistic pathways leading to the corresponding aryl-coupling product (**5**) were investigated (Scheme 4). In the first scenario, the phenyl anion from [PhB(OH)$_2$OEt]$^-$ (ethoxydihydroxyphenylborate) is directly exchanged with the chloride ligand of **4** in a concerted mechanism (Scheme 4A). [PhB(OH)$_2$OEt]$^-$ is formed by reaction of phenyboronic acid and ethanol in basic conditions. Alternatively, a stepwise pathway was examined, in

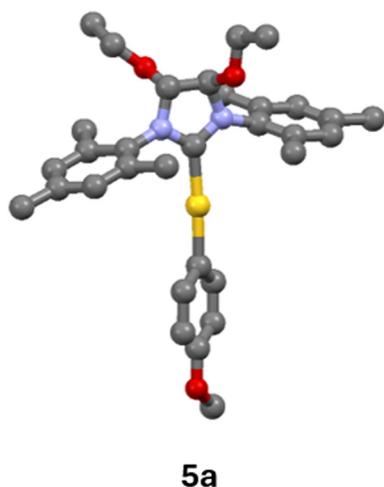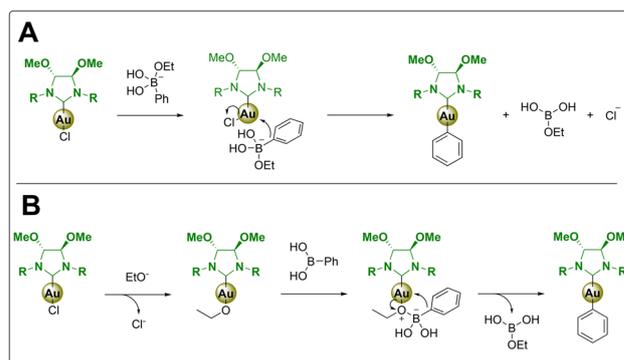**Scheme 4** Concerted mechanism (A) and stepwise mechanism (B) for the reaction of Au(I)–NHC chloride complex **4** with phenylboronic acid (R = 2,6-dimethylphenyl).
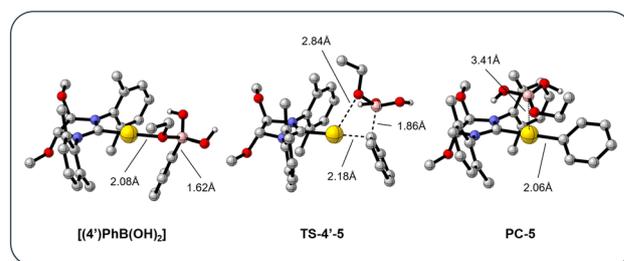

Fig. 4 Stationary points and relevant interatomic distances (in Å) for the coupling step of mechanism D (TS = transition state, PC = product complex). Hydrogen atoms are omitted for clarity. Level of theory: ZORA-BLYP-D3(BJ)/TZ2P.

which the aryl-coupling step is preceded by a ligand exchange equilibrium involving Cl$^-$ and EtO$^-$ at the Au center (Scheme 4B). The net reaction energy was computed to be −37.4 kcal mol^{-1} for both pathways, indicating a thermodynamically favored process. Although in the concerted mechanism the formation of [PhB(OH)$_2$OEt]$^-$ is energetically favored (ΔE_r = −24.3 kcal mol^{-1}) and without appreciable barrier, the kinetic barrier for the coupling step is prohibitively high ($\Delta E^{\ddagger}$ = 32.4 kcal mol^{-1}). Conversely, in the stepwise pathway, both the EtOH$^-$/Cl$^-$ exchange and the gold–aryl coupling steps are relatively facile ($\Delta E^{\ddagger}$ is 12.6 and 12.3 kcal mol^{-1}, respectively). The stationary points for the rearrangement step of **[(4′)PhB(OH)$_2$]** are shown in Fig. 4. These calculations strongly suggest that the stepwise reaction mechanism, proceeding through a metal-borate intermediate, is the kinetically preferred pathway leading to the gold–aryl coupling product **5**.

Synthesis of gold(I)–thiolate complexes bearing backbone functionalized NHCs

As a third class of compounds, we explored NHC–gold(I)–thiolate complexes, a family of species of growing relevance in medicinal chemistry. These complexes can be viewed as auranofin analogues, in which the triethylphosphine ligand of the drug is replaced by an N-heterocyclic carbene, while the thio-

5a

Fig. 3 X-ray molecular structure of complex **5a** is presented, with hydrogen atoms and solvent molecules omitted for clarity.

glucose fragment is substituted by a simpler thiol such as thiophenol. Gold–NHC–thiolate derivatives have recently attracted considerable attention due to their promising antitumor activity, combining the chemical stability and tunability of Au–NHC scaffolds with the biological reactivity of the Au–thiolate fragment.[19,50]

In this work, the target gold(I)-thiolate complexes were efficiently prepared by S–H bond activation of thiophenol or 4-chlorothiophenol in the presence of potassium carbonate and the previously described [Au(NHC)Cl] complexes (**4a–f**) that act as powerful synthons (Scheme 5). The reactions, carried out under aerobic conditions in technical grade ethanol at room temperature for 3 hours, afforded a selection of gold(I)–thiolate complexes (**8a**, **8b**, **8f**, **9b** and **9d**) in excellent yields (87–99%) and high purity after a simple workup, as detailed in the Experimental section (see SI).

Structurally, the resulting compounds are closely related to [IPrAu(SPh)], the only known mononuclear gold(I) complex reported to induce ferroptosis, as mentioned in the Introduction.[19]

The ^{1}H NMR spectra of the newly synthesized complexes show the disappearance of the S–H proton signal of the thiol reagent, together with noticeable shifts of other resonances compared to the parent [Au(NHC)Cl] complex. In the ^{13}C NMR spectra, a signal at high ppm confirms the presence of the carbene carbon bound to gold, along with the expected resonances of both the carbene and aromatic thiolate fragments.

The mechanism of this transformation, previously detailed in our recent work,[34a] proceeds *via* base-assisted deprotonation of the thiol followed by ligand exchange at the gold center
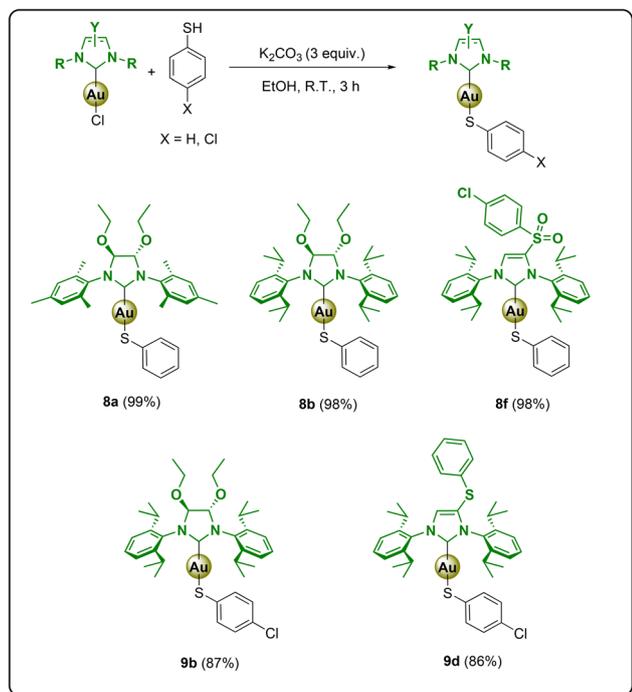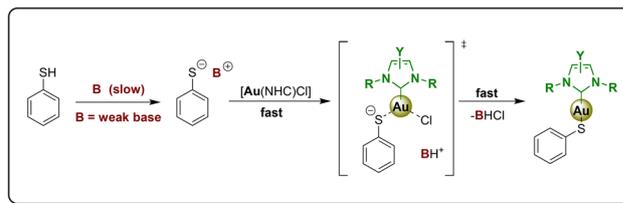
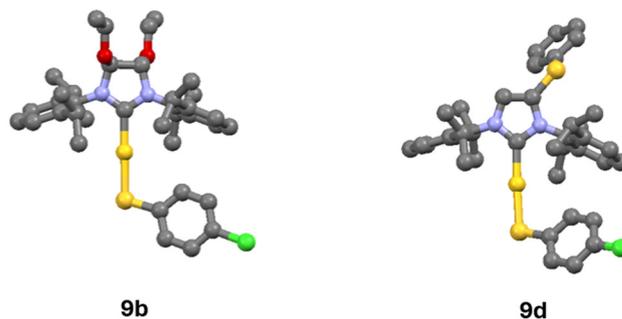**Scheme 6** Proposed mechanism for the synthesis of gold(I)–thiolate complexes.

Fig. 5 X-ray molecular structures of complexes **9b** and **9d** are presented, with hydrogen atoms and solvent molecules omitted for clarity.

(Scheme 6). The thiophenolate anion thus generated readily replaces the chloride ligand, forming the Au–S bond under mild, green, and operationally simple conditions, consistent with the low activation energy associated with this process.

Unequivocal evidence for the formation of the target complexes was obtained from single-crystal X-ray diffraction analyses of suitable crystals of complexes **9b** and **9d**, grown by slow diffusion of *n*-pentane into a chloroform solution of the compound at 4 °C (Fig. 5). The crystallographic analysis confirmed the expected molecular structure, showing an Au–S bond length of approximately 2.29 Å, C–C backbone distances of about 1.53 Å for saturated and 1.38 Å for unsaturated NHCs, a nearly linear C–Au–S angle ranging from 176° to 179°, and an Au–C(carbene) bond length of roughly 2.01 Å. These structural features are in excellent agreement with those reported for related mononuclear Au(I)–NHC–thiolate complexes, further supporting the successful formation and high structural fidelity of the synthesized compounds.

Synthesis of gold(I)–selenolate complexes bearing backbone functionalized NHCs

The final class of compounds investigated in this work comprises gold(I)–selenolate complexes, a family of organometallic species of growing interest due to the unique biological and chemical properties of selenium. Selenium plays an essential role in various biological processes, particularly in the regulation of reactive oxygen species (ROS).[51] Key antioxidant enzymes, such as thioredoxin reductases (TrxR) and glutathione peroxidases (GPx), rely on selenocysteine residues for

Scheme 5 Synthetic route to gold(I)–thiolate complexes.

their catalytic activity. The strategic substitution of sulfur with selenium in the design of new metal-based compounds aims to exploit selenium's distinct biochemical reactivity, with the goal of enhancing therapeutic efficacy while minimizing toxicity and adverse side effects.

The first gold–selenolate complex was reported in the 1990s, motivated by the potential to reduce toxicity relative to the corresponding sulfur analogues.[52] The classical synthetic route involves the reaction of phosphine gold chlorides with selenolates, though such procedures typically require strict inert conditions because of the high air sensitivity of selenols.[53] To overcome this limitation, selenols can be protected through silylation, allowing the synthesis of gold–selenolate complexes under ambient conditions, as demonstrated for dinuclear ferrocene derivatives.[54] Despite these advances, examples of Au–Se bond-containing complexes remain scarce compared to their Au–S counterparts, with most studies focusing instead on gold complexes bearing selenourea ligands.

In this context, we recently reported, in collaboration with the Nolan and Ott groups, the development of two straightforward and versatile synthetic strategies that enable the preparation of gold selenolate complexes under aerobic conditions.[25] The first approach—the *weak-base route*—allows the direct formation of metal–selenolates from [Au(NHC)Cl] precursors and selenophenols, while the second strategy involves the formal selenium insertion into the Au–C bond of gold–aryl complexes. This latter method represents a particularly innovative pathway, as it provides access to gold–selenolate complexes without the need for selenol reagents, relying instead on the reactivity of pre-formed Au–aryl intermediates. The discovery of this unprecedented Se-insertion reactivity expands the synthetic potential of gold–aryl complexes, enabling the conversion of any aryl boron-containing substrate into the corresponding gold–selenolate derivative.

Importantly, *in vitro* biological assays revealed remarkable cytotoxicity of several gold–selenolate complexes toward human cancer cell lines, accompanied by potent inhibition of TrxR activity.[25] One of the complexes exhibited potent cytotoxic activity in advanced 3D tumor organoid models derived from patient tissues, maintaining efficacy even against samples resistant to standard chemotherapeutic agents such as oxaliplatin (colon cancer) and carboplatin (ovarian cancer).

Building upon these findings, in the present work we designed and synthesized two novel gold(ı)–selenolate complexes, following the selenium-insertion strategy applied to gold(ı)–aryl precursors bearing phenyl or 4-trifluoromethyl phenyl fragments.

Specifically, complexes **10b** and **11b** were obtained by direct reaction between gold–aryl complexes **6b/7b** and elemental selenium under argon atmosphere in anhydrous toluene at 110 °C for 24 hours (Scheme 7). At the end of the reaction, the solvent was removed under reduced pressure. Dichloromethane was then added, and the resulting solution was filtered through a PTFE membrane to remove residual gold nanoparticles and unreacted elemental selenium. Precipitation from a dichloromethane/pentane mixture
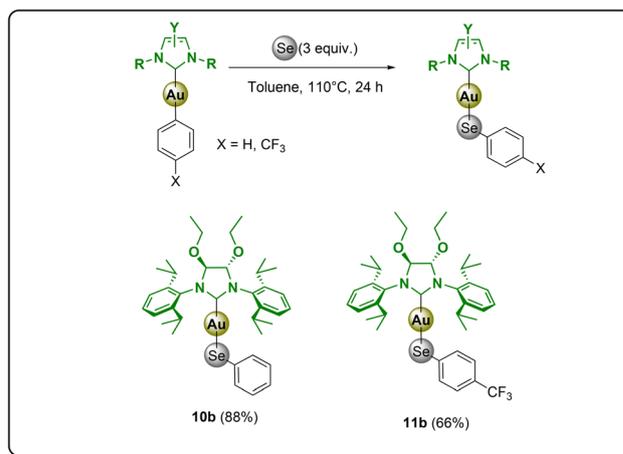
**Scheme 7** Synthetic route to gold(ı)–selenolate complexes.

afforded the pure product as a solid. The isolated compounds **10b** and **11b** were obtained as brownish/orange solids, in 88% and 66% yields, respectively.

To confirm the outcome of the reactions, $^{77}Se\{^1H\}$-NMR spectra were recorded. In both synthesized complexes, a single resonance was detected, indicating the presence of only one selenium-containing species in solution. Moreover, the chemical shifts of these signals (92 ppm for the phenyl derivative and 113 ppm for the more electron-poor 4-trifluoromethyl-phenyl analogue) closely match those reported in our recent work, which are characteristic of an aryl–selenolate ligand coordinated to gold(ı).

The ^1H and ^{13}C NMR spectra exhibit only minor shifts compared to the parent gold(ı)–aryl complexes, while maintaining the same number of resonances, as no change in the number of hydrogen or carbon atoms occurs during the selenium insertion process.

An aspect that remained unexplored in our previous study concerns the mechanistic pathway of selenium insertion into the Au–aryl bond.

To gain insight into the mechanistic pathway of Se insertion, the reaction of precursor **5** was investigated *in silico* at the same level of theory adopted for the gold–aryl coupling reaction. Given that the synthesis of gold(ı)–selenolate derivatives proceeds slowly despite heating, the reaction mechanism depicted in Scheme 8 was proposed. Monoatomic Se is gradually formed by dissolution of its solid elemental form. Although this is a simplification introduced to facilitate com-
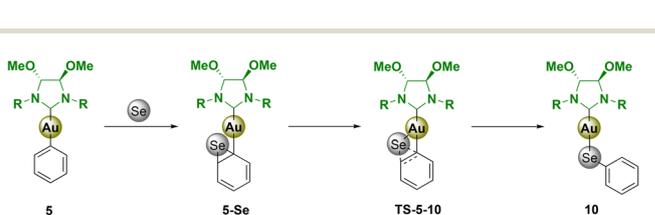
Scheme 8 Insertion reaction of Se with Au(ı)-phenyl complex **5** (R = 2,6-dimethylphenyl) (TS = transition state).
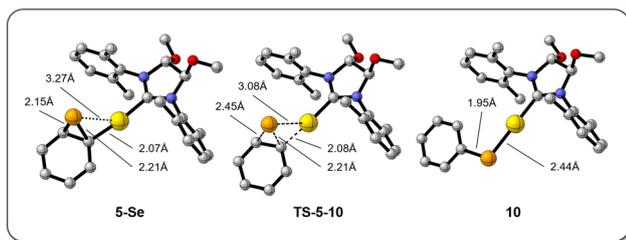
Fig. 6 Stationary points and relevant interatomic distances (in Å) for the insertion of Se in complex **5** (TS = transition state). Hydrogen atoms are omitted for clarity. Level of theory: ZORA-BLYP-D3(BJ)/TZ2P.

putational modelling, since it is extremely difficult to establish experimentally the actual selenium species involved, we consider monoatomic Se as a reasonable representation of the reactive species that initially interacts with **5** by engaging the phenyl ligand, which has a partial anionic character, to form the energetically-favoured π-adduct **5**-Se ($\Delta E_{5\text{-Se}} = -18.0$ kcal mol^{-1}). The subsequent insertion of Se into the Au–C bond occurs through the interaction with the metal center (**TS-5–10**, Fig. 6) and results in the reduction of Se^0 to the selenide (-2) oxidation state. The overall reaction is significantly exergonic ($\Delta E_r = -69.5$ kcal mol^{-1}) and proceeds with a modest activation energy ($\Delta E^{\ddagger} = 3.3$ kcal mol^{-1}), suggesting that the conversion rates are limited by the sluggish dissolution of Se from the solid phase into the toluene reaction mixture.

Stability, solubility and lipophilicity studies

After the synthesis of the gold(I)–NHC complexes of interest, we proceeded to their biological evaluation. As an initial step, preliminary studies were carried out to assess the stability and solubility of the complexes in solution before moving to cellular assays.

The stability of the newly synthesized gold(I) complexes was first evaluated in a 1 : 1 D$_2$O/DMSO-d$_6$ mixture by NMR spectroscopy. Over 48 hours, the spectra remained unchanged, indicating that the complexes retained their structural integrity under these conditions.

Since the pharmacokinetic behavior of metal-based drugs is strongly influenced by their solubility and tendency to aggregate, these properties were further investigated using dynamic light scattering (DLS). Stock solutions (20 mM in DMSO) were diluted with PBS to a final concentration of 100 μM, and particle size distributions were recorded immediately. Most complexes showed good solubility and remained molecularly dispersed; however, a few derivatives exhibited signs of nanoparticle or aggregate formation.

For these compounds, the concentration was progressively reduced to 1 μM. Complexes that remained poorly soluble or aggregation-prone even at this lowest concentration (**4c**, **4d**, **4f**, **5b**, **6d** and **10b**) were excluded from further biological evaluation.

The lipophilicity of a compound is a key parameter in drug design, influencing its cell membrane permeability, distri-

Table 1 Distribution coefficients (log P) of the newly synthesized gold(I) complexes against octanol and phosphate-buffered saline. All data are presented as mean $\pm$ standard deviation

Compound	log P
4a	0.090 ± 0.002
4b	0.13 ± 0.02
4e	0.14 ± 0.03
5a	0.22 ± 0.02
5d	1.14 ± 0.08
5f	0.44 ± 0.07
6b	0.16 ± 0.02
7b	0.68 ± 0.04
7d	0.93 ± 0.06
8a	0.7 ± 0.2
8b	0.55 ± 0.23
8f	0.21 ± 0.04
9b	0.15 ± 0.02
9d	1.09 ± 0.03
11b	1.15 ± 0.06

bution, and overall biological efficacy, particularly in the case of metallodrugs. To evaluate this property for our gold(I) complexes, the classical shake-flask method was employed.[55] This technique determines the octanol–water partition coefficient (log P) by measuring the distribution of each compound between 1-octanol and phosphate buffer (pH 7.4). UV–visible spectroscopy was used to quantify the concentration in each phase.

The log P value was calculated based on the relative absorbance intensities in the two immiscible phases: I_o representing the octanol-rich layer and I_w corresponding to the water-rich layer (Table 1). This parameter serves as a measure of the compound's preference for hydrophilic or lipophilic environments: negative values indicate hydrophilicity, positive values reflect lipophilicity, and values near zero suggest a balanced affinity for both phases.

Among the compounds analysed, three distinct lipophilicity ranges were identified: (i) moderate lipophilicity (log P between 0.09 and 0.22, as in the case of complexes **4a–c**, **5a**, **6b**, **8f** and **9b**), (ii) good lipophilicity (log P between 0.44 and 0.70, as in the case of complexes **5f**, **7b**, **8a–b**) and (iii) high lipophilicity (log P between 0.93 and 1.15, as in the case of complexes **5d**, **7d**, **9d** and **11b**).

These preliminary lipophilicity data provide important insights into the physicochemical profiles of the complexes and will serve, at least partially, to rationalize trends observed in anticancer activity on tumor cell models.

Antiproliferative activity on cancer and non-cancerous cells

The cytotoxicity of the newly synthesized gold(I) complexes was evaluated on three representative tumor cell lines: CT-26 (colon carcinoma), MCF-7 (breast adenocarcinoma), and PT-45 (pancreatic carcinoma). These cell lines were selected to provide a broad overview of anticancer activity across biologically and clinically distinct tumor types. Colon carcinoma, represented by CT-26 cells, is one of the most common and lethal gastrointestinal cancers, often characterized by high prolifer-

ation rates and chemoresistance.[56] Breast adenocarcinoma, modeled by MCF-7 cells, represents a prevalent hormone-dependent tumor with well-established *in vitro* models for drug screening.[57] Pancreatic carcinoma, represented by PT-45 cells, is particularly aggressive and notoriously difficult to treat, making it a critical target for the evaluation of novel chemotherapeutics.[58] Together, these three cell lines offer a diverse spectrum of tumor biology, allowing us to assess the compounds' efficacy against cancers with very different cellular behaviors and therapeutic challenges.

This strategy not only allows a general assessment of cytotoxic potential but also enables direct comparison with the reference chemotherapeutic cisplatin and with previously reported gold complexes bearing non-functionalized NHC ligands studied by our team.[10] To further explore selectivity toward tumor cells, the complexes were also tested on a non-tumoral human embryonic kidney cell line (HEK-293).

Cytotoxicity was measured using the MTT assay, with the same number of cells seeded in each well and treated with compound concentrations ranging from 0.01 μM to 100 μM. The resulting IC_{50} values, representing the concentration required to inhibit 50% of the cell population, provide a quantitative measure of the compounds' cytotoxic potency and are reported in Table 2.

Across the three cancer cell lines investigated (CT-26, MCF-7, and PT-45), the overall trends in cytotoxicity are broadly consistent, indicating that the biological response is primarily governed by structural features of the complexes rather than strong cell-line-specific effects. The most potent derivatives—notably **4a**, **4b**, and **4e**—rank among the top performers in all models, with **4b** displaying markedly enhanced activity. Although some quantitative differences in sensitivity are observed (likely reflecting variations in cellular uptake,

metabolism, or redox state among the lines), no pronounced selectivity toward a single cancer type emerges.

A clearer structure–activity relationship becomes apparent when the data are analysed according to ligand environment rather than biological model. Au(I)–Cl complexes constitute the most active class overall, followed by Au(I)–SPh and Au(I)–aryl(4-OMe) derivatives, whereas Au(I)–aryl(4-CF$_3$), Au(I)–SPh(4-Cl), and Au(I)–Se-aryl(4-CF$_3$) complexes display poor activity. Notably, the cytotoxicity data indicate that Au(I)–SPh complexes exhibit activity comparable to [Au(IPr)(SPh)] and slightly lower than auranofin.

Within both the Au(I)–aryl(4-X) and Au(I)–SPh(4-X) series, derivatives bearing electron-donating substituents or hydrogen in the *para* position consistently outperform those containing electron-withdrawing groups. This trend indicates that electronic effects at the ancillary ligand influence biological performance, plausibly through modulation of Au–ligand bond polarization, ligand lability, and accessibility of the metal centre to biomolecular targets. The decrease in activity observed upon introduction of strongly withdrawing substituents (*e.g.*, **5d** *vs.* **7d** or **8b** *vs.* **9b**) supports this interpretation.

The nature of the NHC ligand also contributes significantly to cytotoxic behaviour. Oxygen-based NHCs generally confer higher cytotoxicity than sulfur-based analogues (*e.g.*, **4b** *vs.* **4d** or **5b** *vs.* **5d**), and sulfone-containing ligands appear more effective than the corresponding thioether congeners (*e.g.*, **5d** *vs.* **5f**). These observations suggest that both electronic and steric factors are relevant: heteroatom substitution modifies σ-donor strength and polarization of the Au–C bond, while also altering steric profile and hydrogen-bonding capability, thereby affecting interactions with biological media. Experimental measurements and DFT calculations confirm a donor strength trend of oxygen-based NHCs > sulfur-based NHCs > sulfone-based NHCs. While the most strongly donating oxygen-based carbenes usually correspond to the most active complexes, the correlation between carbene donor ability and cytotoxicity is not monotonic: sulfone-based NHCs, despite being the weakest donors, display intermediate activity, indicating that cytotoxicity results from a multifactorial balance that also includes steric accessibility, ancillary ligand effects, and physicochemical transport parameters.

Comparison with previously studied systems bearing the non-functionalized IPr ligand further indicates that backbone saturation and incorporation of oxygen-based substituents enhance the efficacy of Au(I)–Cl and Au(I)–SPh complexes, whereas similar modifications appear detrimental for Au(I)–selenolate derivatives, as exemplified by the inactivity of complex **11b** relative to both its aryl precursor and the corresponding IPr analogue.

Lipophilicity remains an important but not exclusive determinant of activity. The most potent compounds typically exhibit moderate log P values (<0.7), consistent with a favourable hydrophilic–lipophilic balance that promotes cellular uptake while maintaining aqueous compatibility. However, this trend should be interpreted within a broader physicochemical framework: lipophilicity reflects not only substituent

Table 2 Cytotoxicity of gold(I) complexes toward cancer and non-cancerous cells

IC_{50} (μM)

	CT-26	MCF-7	PT-45	HEK-293
Cisplatin	16 ± 2	18 ± 3	6.4 ± 0.3	2.1 ± 0.2
Auranofin[59]	0.92 ± 0.06	1.8 ± 0.1	—	—
[Au(IPr)Cl][10]	18 ± 3	16 ± 3	32 ± 4	6.8 ± 0.5
4a	4.8 ± 0.2	6.7 ± 0.2	2.41 ± 0.06	3.3 ± 0.5
4b	0.7 ± 0.2	6.6 ± 0.4	1.35 ± 0.04	1.73 ± 0.06
4e	2.2 ± 0.4	3.4 ± 0.2	1.31 ± 0.01	1.9 ± 0.2
[Au(IPr)(4-OMe-Ph)][10]	13 ± 3	9 ± 1	21 ± 6	5 ± 2
5a	5.2 ± 0.4	2.2 ± 0.5	1.6 ± 0.2	3.7 ± 0.9
5d	48 ± 6	25 ± 1	9.0 ± 0.5	10 ± 1
5f	13 ± 1	15 ± 1	5.0 ± 0.3	3.8 ± 0.4
6b	>20	3 ± 2	5 ± 2	>20
7b	28 ± 10	13 ± 4	8 ± 2	26 ± 19
7d	>100	>100	>100	>100
[Au(IPr)(SPh)][10]	5 ± 2	5 ± 2	9 ± 1	11.3 ± 0.9
8a	6.4 ± 0.2	2.15 ± 0.04	2.56 ± 0.04	6.3 ± 0.6
8b	8.4 ± 2.5	4 ± 2	5.9 ± 0.1	3.5 ± 0.2
8f	20 ± 14	20 ± 1	16 ± 10	25 ± 4
9b	23 ± 4	20 ± 12	>100	>100
9d	>100	>100	>100	>100
[Au(IPr)(SePh)][10]	—	48 ± 5	—	—
11b	>100	>100	>100	>100

hydrophobicity but also the interplay between hydrophobic volume of the NHC wingtip groups and the polar contribution of heteroatoms within the backbone. Excessively high lipophilicity (>0.9) correlates with significantly reduced activity, rendering complexes **5d**, **7d**, **9d** and **11b** poorly active or inactive.

Importantly, the present data indicate that electronic characteristics of ligands and steric environment around the metal centre also influence biological response, demonstrating that cytotoxicity arises from a multifactorial balance of donor properties, ligand lability, steric accessibility, and physicochemical transport parameters rather than from lipophilicity alone.

The cytotoxicity evaluation in non-cancerous HEK-293 cells reveals only limited selectivity for most derivatives, including cisplatin, highlighting that further optimization will require tuning of both physicochemical and electronic ligand parameters to improve therapeutic windows.

Taken together, the cytotoxicity results identify complex **4b** as the most promising candidate, exhibiting the highest activity among all tested compounds. Notably, **4b** is significantly more active than its analogue bearing the non-functionalized IPr ligand ([Au(IPr)Cl]) as well as than aryl, thiolate, and selenolate complexes containing the same saturated oxygen-based NHC ligand. Importantly, the cytotoxicity of **4b** is comparable to literature-reported IC_{50} values for auranofin in relevant cancer cell lines (see Table 2), highlighting its potent antiproliferative profile. These results make **4b** an ideal candidate for further in-depth studies aimed at elucidating its mechanism of action.

To this end, and to distinguish between cytostatic and cytotoxic effects, cell viability was further evaluated using two complementary fluorescent dyes: Calcein-AM and Propidium Iodide (PI). Calcein-AM is a cell-permeable dye that enters both live and dead cells; however, in viable cells, intracellular esterases cleave the acetomethoxy (AM) group, generating a green fluorescent signal indicative of living cells (Fig. 7).[60] In contrast, PI is a membrane-impermeable dye that can only enter cells with compromised membranes.[61] Upon binding to DNA, PI emits red fluorescence, marking non-viable cells.

Cells treated with compound **4b** displayed strong red fluorescence, demonstrating that the compound induces cell death rather than merely inhibiting proliferation (Fig. 7). These results indicate that **4b** exerts a cytotoxic effect, confirming its ability to actively reduce cell viability rather than producing a cytostatic arrest.

ROS generation

The production of reactive oxygen species (ROS) was assessed using the cell-permeable fluorescent probe 2′,7′-dichlorodihydrofluorescein diacetate (H_2DCFDA).[62] Upon entering the cell, intracellular esterases cleave the acetate groups, converting H_2DCFDA into the non-fluorescent compound H_2DCF. In the presence of ROS, H_2DCF is oxidized to 2′,7′-dichlorofluorescein (DCF), a highly fluorescent molecule emitting green light, thereby providing a direct measure of intracellular ROS levels. Notably, the dye H_2DCFDA is not able to differentiate between the different types of ROS inside a cellular environment.[63]

The experiment was performed in CT-26 colon carcinoma cells, using H_2DCFDA at a concentration of 15 μM with a 4-hour incubation period, while complex **4b** was administered at its IC_{50} value (0.7 μM) for 48 hours (Fig. 8). Hydrogen peroxide (H_2O_2) was included as a positive control due to its well-established ability to generate radical species. In control wells treated only with the probe, minimal fluorescence was observed. In contrast, cells exposed to H_2O_2 exhibited intense green fluorescence, confirming ROS generation. Similarly, treatment with complex **4b** induced strong green fluorescence, indicating a substantial increase in intracellular oxidative stress. As H_2DCFDA is a general ROS indicator, these results reflect an overall elevation in ROS levels rather than the formation of specific reactive oxygen species.

Lipid peroxidation

A key hallmark of ferroptosis is the oxidation of polyunsaturated fatty acids in cellular membranes by reactive oxygen species, particularly hydroxyl radicals, leading to the formation of highly cytotoxic lipid peroxides.[64–67] Monitoring lipid peroxidation is therefore crucial to confirm ferroptotic cell death, as it provides direct evidence of the oxidative damage driving this pathway.

Lipid peroxidation was evaluated using the fluorescent probe BODIPY™ 581/591 C11, a highly sensitive reporter that integrates into cellular membranes and exhibits a distinct shift in fluorescence emission upon oxidation by lipid per-
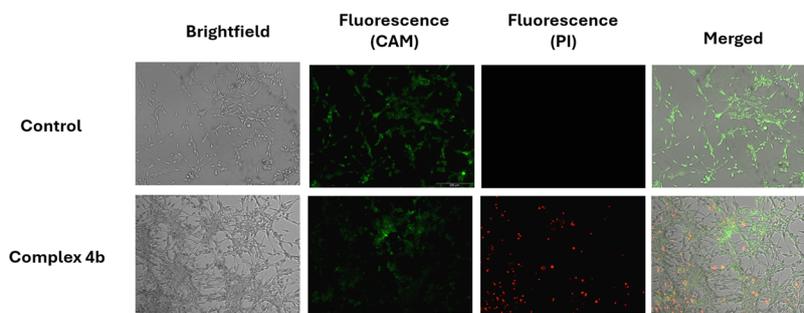

Fig. 7 Cell viability images were recorded with a 10× objective and 1× ocular. Calcein AM λ_{ex} = 460–490 nm, λ_{em} = 517 nm. Propidium iodide λ_{ex} = 545–580 nm, λ_{em} = 617 nm. Scale bar: 200 μm.
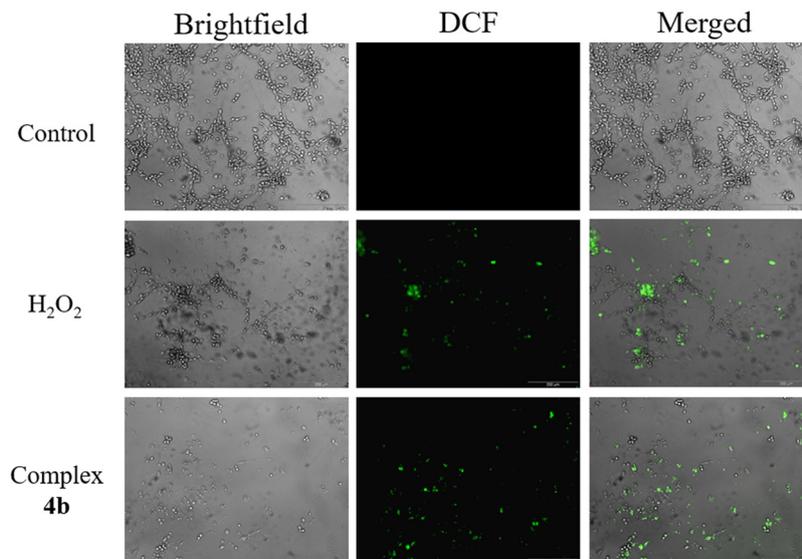
Fig. 8 Fluorescence microscopy images of CT-26 cells upon co-incubation with **4b** (0.7 μM) and ROS-specific probe 2′,7′-dichlorodihydrofluorescein diacetate (λ_{ex} = 460–490 nm, λ_{em} = 517–527 nm). Scale bar: 200 μm.

oxides.[68] This property enables real-time detection and quantification of oxidative damage within lipid bilayers in live cells.

Treatment of cells with complex **4b** for 24 hours resulted in a marked accumulation of lipid peroxides, as revealed by the BODIPY™ 581/591 probe (Fig. 9). These results confirm that **4b** triggers lipid peroxidation, providing strong evidence that the cytotoxic effects of the compound involve ferroptotic mechanisms. The combination of ROS generation, GSH depletion, and now lipid peroxidation collectively supports the notion that **4b** exerts its anticancer activity, at least in part, through the induction of ferroptosis.

Glutathione depletion

Another key early marker for ferroptotic and oxidative stress-related cell death is the depletion of intracellular glutathione (GSH).[69] During ferroptosis, glutathione peroxidase 4 (GPX4) reduces lipid peroxides to their corresponding alcohols using electrons donated by GSH, leading to a progressive depletion of intracellular GSH levels. Monitoring GSH levels can therefore provide important insights into oxidative stress-mediated cell death pathways.

Intracellular GSH was assessed using ThiolTracker™ Violet, a bright fluorescent probe that selectively reacts with free thiol groups, such as those present in GSH, forming a highly emissive adduct upon binding.[70] Treatment with complex **4b** for 4 hours resulted in a marked reduction in intracellular GSH, indicating disruption of the cellular redox balance (Fig. 10).

To achieve higher spatial resolution and capture detailed cellular responses, the samples were also analysed by confocal microscopy, which allows the acquisition of three-dimensional image stacks while eliminating out-of-focus light.

The merged images revealed that a substantial fraction of cells treated with **4b** exhibited complete depletion of GSH, accompanied by irreversible membrane damage and clear morphological signs of cell death, including leakage of organelles and elongated or distorted cell shapes (Fig. 11). In addition, a smaller portion of the population showed intermediate effects, with partial GSH loss, early lipid peroxidation,
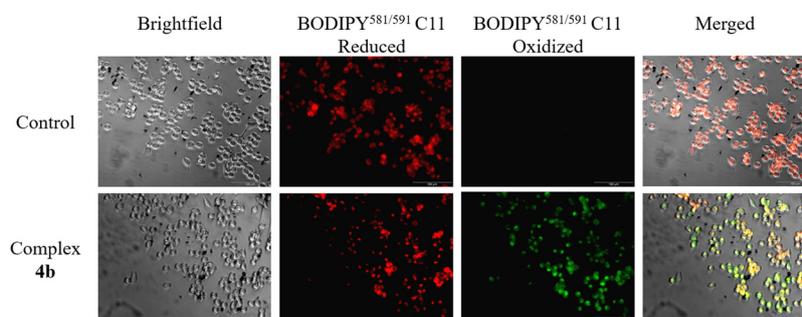

Fig. 9 Fluorescence microscopy images upon co-incubation of **4b** with the LPO-specific probe BODIPY[581/591] C11. Red channel: reduced dye (λ_{ex} = 530–550 nm, λ_{em} = 590 nm − LP); green channel: oxidized dye (λ_{ex} = 460–490 nm, λ_{em} = 510–550 nm). Scale bar: 100 μm.
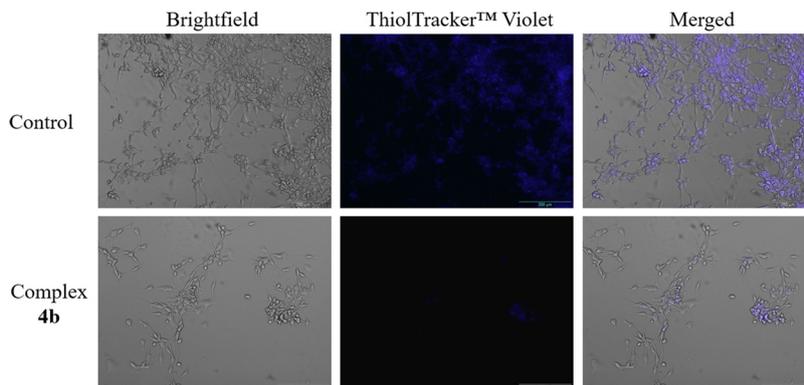
Fig. 10 Fluorescence microscopy images of CT-26 cells upon co-incubation with **4b** (0.7 μM) and the GSH-specific probe ThiolTracker™ Violet (λ_{ex} = 330–385 nm, λ_{em} = 420 nm − LP). Scale bar: 200 μm.
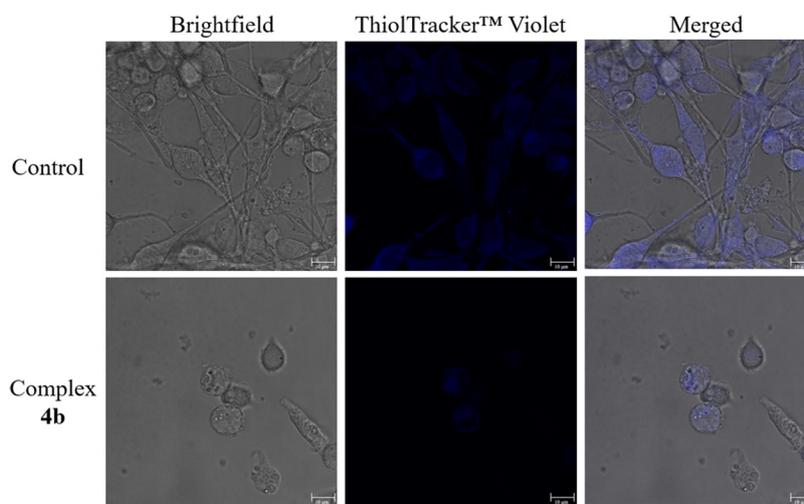

Fig. 11 Confocal laser scanning microscopy of CT-26 cells upon co-incubation with **4b** (0.7 μM) and the GSH-specific probe ThiolTracker™ Violet (λ_{ex} = 405 nm, λ_{em} = 525 nm). Scale bar: 10 μm.

and morphological alterations, while only a minor fraction of cells remained largely unaffected, retaining high GSH levels and normal morphology.

These observations demonstrate that complex **4b** not only promotes ROS production but also disrupts intracellular antioxidant defenses, providing strong evidence that it induces cell death through oxidative stress-mediated mechanisms, potentially involving both ferroptotic and apoptotic pathways. While GSH depletion represents an important early event in ferroptosis, it is not by itself sufficient to conclusively establish ferroptotic cell death, as GPX4 activity is a central determinant in this process. Notably, in our previous study,[19] structurally related compounds were shown to induce ferroptosis accompanied by GPX4 downregulation. In combination with the present observations of lipid peroxidation, the depletion of intracellular GSH observed here is therefore consistent with ferroptosis as a major contributing mechanism of cell death.

Cell fluorescent imaging of intracellular Fe²⁺

A final and highly informative test for confirming ferroptosis involves the measurement of intracellular Fe^{2+} levels. Despite its critical relevance, this assay has been scarcely reported in studies of ferroptosis induced by metallodrugs. However, we consider it important for achieving molecular-level precision in assessing ferroptotic induction.

Iron is the most abundant transition metal in living organisms and plays pivotal roles in numerous physiological processes.[71] Within cells, free iron exists primarily in two redox states, ferrous (Fe^{2+}) and ferric (Fe^{3+}), with Fe^{2+} being particularly significant under the reducing conditions of the intracellular environment. Its high solubility, reactivity, and interactions with metal transporters make Fe^{2+} a central player in iron-mediated biochemical processes.

As previously mentioned, ferroptosis is defined as a non-apoptotic cell death pathway driven by the iron-dependent
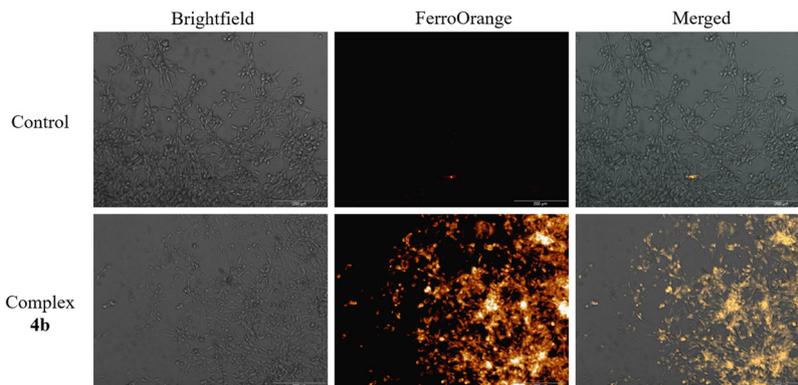
Fig. 12 Fluorescence microscopy images of CT-26 cells upon co-incubation with **4b** (0.7 μM) and the labile Fe^{2+}-specific probe FerroOrange (λ_{ex} = 542 nm, λ_{em} = 572 nm). Scale bar: 200 μm.
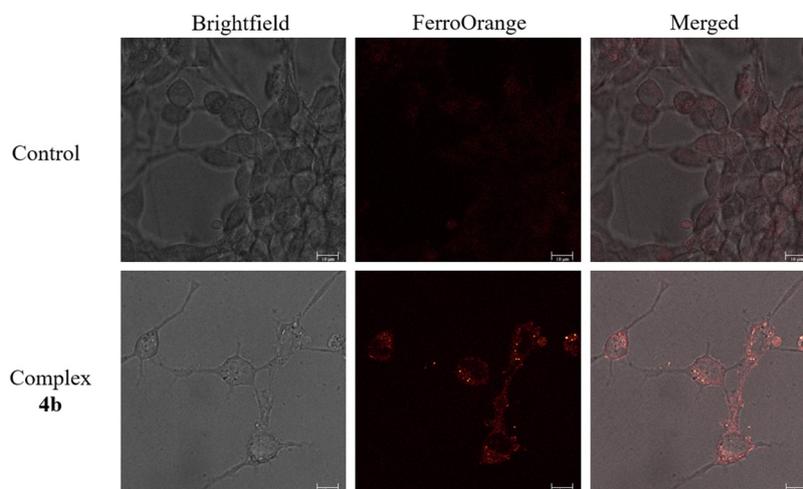

Fig. 13 Confocal laser scanning microscopy of CT-26 cells upon co-incubation of **4b** (0.7 μM) and the labile Fe^{2+}-specific probe FerroOrange (λ_{ex} = 542 nm, λ_{em} = 572 nm). Scale bar: 10 μm.

accumulation of lipid peroxides, and biochemical processes mediated by iron accumulation are considered a hallmark of this form of cell death. Accurate monitoring of intracellular Fe^{2+} levels is therefore essential to confirm and understand the progression of ferroptosis. A marked increase in detectable Fe^{2+} reflects a disruption of iron metabolism, providing strong molecular evidence for ferroptotic cell death.

In our study, the intracellular distribution of Fe^{2+} was analysed using both conventional fluorescence (FL) microscopy and confocal microscopy (Fig. 12 and 13, respectively).[72]

While FL microscopy allowed rapid visualization of Fe^{2+}-rich regions across the cell population, confocal microscopy provided high-resolution three-dimensional imaging, eliminating out-of-focus light and revealing subcellular localization with greater precision. The combination of these two complementary techniques ensures robustness and reliability of the results, minimizing artifacts and confirming that the observed Fe^{2+} accumulation is genuine. Bright intracellular spots were observed, corresponding to Fe^{2+} localized within specific organelles.

These findings not only confirm the iron-dependent mechanism of ferroptosis induced by our selected gold(I) complex, but also represent, to our knowledge, the most detailed and rigorous study currently available in the literature on ferroptosis driven by antitumor gold(I) complexes, thanks to the use of complementary imaging approaches.

Conclusions

In summary, we have reported the design, synthesis, and comprehensive evaluation of 21 novel gold(I) complexes bearing backbone-functionalized NHC ligands, encompassing chloride, thiolate, aryl, and selenolate derivatives. The work presented herein highlights not only the versatility and robustness of our synthetic strategies, but also the careful mechanistic elucidation underlying each transformation, from azolium salt formation to the generation of structurally diverse gold(I) species. In particular, the weak-base approach allowed efficient and scalable access to [Au(NHC)Cl] complexes, while sub-

sequent thiol, aryl, and selenium insertions proceeded under mild, operationally simple, and environmentally benign conditions. Detailed NMR and single-crystal X-ray analyses confirmed the structural integrity and stereoelectronic features of all complexes, while DFT studies provided molecular-level insights into the mechanistic pathways, particularly for the gold–aryl and selenium-insertion reactions. Importantly, both saturated and unsaturated azolium salts/NHCs efficiently afforded the target gold(I) complexes, indicating that this structural variation does not significantly impact metalation efficiency or complex stability.

Beyond synthetic and mechanistic rigor, our work systematically explored the biological potential of these gold(I) complexes as ferroptosis inducers. Comprehensive cellular assays demonstrated that select complexes, notably **4b**, exhibit potent cytotoxicity across multiple human cancer cell lines, outperforming cisplatin in several models. Using complementary fluorescence-based techniques, we directly linked their antitumor activity to hallmark features of ferroptosis: reactive oxygen species (ROS) generation, glutathione depletion, lipid peroxidation, and intracellular Fe^{2+} accumulation. The simultaneous occurrence of these key biochemical events reflects a canonical ferroptotic signature and closely parallels the biological profile previously observed for our cobalt(III) and gold(I) reference complexes studied under the same experimental conditions,[19,66] where ferroptosis was demonstrated to represent the dominant—though not exclusive—cell death pathway. Moreover, confocal microscopy provided high-resolution spatial mapping of these processes, revealing, for the first time with such molecular precision, the iron-dependent mechanism of cell death induced by a gold(I)–NHC complex. These findings underscore the critical role of NHC backbone functionalization in modulating both the electronic properties of the gold center and the resulting biological activity, offering clear structure–activity relationships that can guide the rational design of next-generation metallodrugs.

Taken together, this study represents a holistic approach to metallodrug development, combining meticulous synthetic methodology, mechanistic understanding, and rigorous biological evaluation. The gold(I) complexes described here not only expand the chemical space of functionalized NHC ligands but also provide unprecedented insight into the molecular underpinnings of ferroptosis induction, establishing a foundation for future therapeutic exploration.

Conflicts of interest

The authors declare no competing interests.

Data availability

The datasets supporting this article have been uploaded as part of the supplementary information (SI). Supplementary information is available. See DOI: **https://doi.org/10.1039/d6qi00134c**.

CCDC 2518319–2518330 contain the supplementary crystallographic data for this paper.[73a–l]

Acknowledgements

References

1 E. J. Anthony, E. M. Bolitho, H. E. Bridgewater, O. W. L. Carter, J. M. Donnelly, C. Imberti, E. C. Lant, F. Lermyte, R. J. Needham, M. Palau, P. J. Sadler, H. Shi, F.-X. Wang, W.-Y. Zhang and Z. Zhang, Metallodrugs are unique: opportunities and challenges of discovery and development, *Chem. Sci.*, 2020, **11**, 12888–12917.

2 A. Casini and A. Pöthig, Metals in Cancer Research: Beyond Platinum Metallodrugs, *ACS Cent. Sci.*, 2024, **10**, 242–250.

3 M. E. Hoffmann and F. E. Kühn, Au NHC complexes as anticancer agents: milestones, strategies and future developments, *Chem. Soc. Rev.*, 2025, **54**, 10326–10343.

4 Q. Zhao, B. Han, C. Peng, N. Zhang, W. Huang, G. He and J. Li, A promising future of metal–N–heterocyclic carbene complexes in medicinal chemistry: The emerging bioorganometallic antitumor agents, *Med. Res. Rev.*, 2024, **44**, 2194–2235.

5 T. Scattolin, A. A. Logvinov, N. V. Tzouras, C. S. J. Cazin and S. P. Nolan, Advances in the Synthesis and Applications of N-Heterocyclic Carbene Metal Complexes with a Focus on the Weak Base Route, *Organometallics*, 2023, **42**, 2692–2730.

6 E. Zampieri, C. Donati, V. Mechrouk, T. Achard, S. Bellemin-Laponnaz, A. Dolmella, C. Marzano, M. Baron,

V. Gandin and C. Tubaro, Gold(ı) complexes with NHC ligands functionalized with sulfoxide groups: Design, synthesis, in vitro studies and insights into the mechanism of action as anticancer drugs, *J. Inorg. Biochem.*, 2025, **271**, 112957.

7 R. De Marco, V. Giuso, T. Achard, M. Rancan, M. Baron, L. Armelao, M. Mauro, S. Bellemin-Laponnaz and C. Tubaro, Exploring the coordination properties of Phosphonium–Functionalized N–Heterocyclic carbenes towards gold, *Eur. J. Inorg. Chem.*, 2023, **26**, e202300184.

8 L. Benhamou, N. Vujkovic, V. César, H. Gornitzka, N. Lugan and G. Lavigne, Facile derivatization of a "Chemo-active" NHC incorporating an enolate backbone and relevant tuning of its electronic properties, *Organometallics*, 2010, **29**, 2616–2630.

9 L. Benhamou, V. César, H. Gornitzka, N. Lugan and G. Lavigne, Imidazol-2-ylidene-4-olate: an anionic N-heterocyclic carbene pre-programmed for further derivatization, *Chem. Commun.*, 2009, 4720.

10 D. V. Pasyukov, M. A. Shevchenko, K. E. Shepelenko, O. V. Khazipov, J. V. Burykina, E. G. Gordeev, M. E. Minyaev, V. M. Chernyshev and V. P. Ananikov, One–Step Access to Heteroatom–Functionalized Imidazol(in)ium Salts, *Angew. Chem., Int. Ed.*, 2021, **61**, e202116131.

11 R. P. Herrera and M. C. Gimeno, Main avenues in gold coordination Chemistry, *Chem. Rev.*, 2021, **121**, 8311–8363.

12 I. Ott, On the medicinal chemistry of gold complexes as anticancer drugs, *Coord. Chem. Rev.*, 2009, **253**, 1670–1681.

13 G. Moreno-Alcántar, P. Picchetti and A. Casini, Gold complexes in anticancer therapy: From new design principles to Particle–Based delivery systems, *Angew. Chem., Int. Ed.*, 2023, **262**, e202218000.

14 J. L. Hickey, R. A. Ruhayel, P. J. Barnard, M. V. Baker, S. J. Berners-Price and A. Filipovska, Mitochondria-Targeted Chemotherapeutics: The rational design of Gold (ı) N-Heterocyclic carbene complexes that are selectively toxic to cancer cells and target protein selenols in preference to thiols, *J. Am. Chem. Soc.*, 2008, **130**, 12570–12571.

15 R. Rubbiani, E. Schuh, A. Meyer, J. Lemke, J. Wimberg, N. Metzler-Nolte, F. Meyer, F. Mohr and I. Ott, TrxR inhibition and antiproliferative activities of structurally diverse gold N-heterocyclic carbene complexes, *MedChemComm*, 2013, **4**, 942.

16 A. Citta, E. Schuh, F. Mohr, A. Folda, M. L. Massimino, A. Bindoli, A. Casini and M. P. Rigobello, Fluorescent silver (ı) and gold(ı)–N-heterocyclic carbene complexes with cytotoxic properties: mechanistic insights, *Metallomics*, 2013, **5**, 1006.

17 E. Schuh, C. Pflüger, A. Citta, A. Folda, M. P. Rigobello, A. Bindoli, A. Casini and F. Mohr, Gold(ı) carbene complexes causing thioredoxin 1 and thioredoxin 2 oxidation as potential anticancer agents, *J. Med. Chem.*, 2012, **55**, 5518–5528.

18 S. M. Mahdavi, D. Bockfeld, I. V. Esarev, P. Lippmann, R. Frank, M. Brönstrup, I. Ott and M. Tamm, Gold(ı) and gold(ııı) carbene complexes from the marine betaine nor-zooanemonin: inhibition of thioredoxin reductase, antiproliferative and antimicrobial activity, *RSC Med. Chem.*, 2024, **15**, 3248–3255.

19 E. Schlegel, Z. Papadopoulos, N. Montesdeoca, V. A. Voloshkin, S. P. Nolan, S. A. Hahn, T. Scattolin and J. Karges, Gold(ı) N-Heterocyclic carbene complexes as ferroptosis inducing anticancer agents, *ACS Med. Chem. Lett.*, 2025, **16**, 856–864.

20 T. Scattolin, G. Tonon, E. Botter, S. G. Guillet, N. V. Tzouras and S. P. Nolan, Gold(ı)–N–Heterocyclic carbene synthons in organometallic synthesis, *Chem. – Eur. J.*, 2023, **29**, e202301961.

21 (a) S. J. Dixon and J. A. Olzmann, The cell biology of ferroptosis, *Nat. Rev. Mol. Cell Biol.*, 2024, **25**, 424–442; (b) S. Li, H. Yuan, Y. Chen and Z. Guo, Metal complexes induced ferroptosis for anticancer therapy, *Fundam. Res.*, 2022, **3**, 525–528.

22 L. F. Boullosa, J. Van Loenhout, T. Flieswasser, J. De Waele, C. Hermans, H. Lambrechts, B. Cuypers, K. Laukens, E. Bartholomeus, V. Siozopoulou, W. H. De Vos, M. Peeters, E. L. J. Smits and C. Deben, Auranofin reveals therapeutic anticancer potential by triggering distinct molecular cell death mechanisms and innate immunity in mutant p53 non-small cell lung cancer, *Redox Biol.*, 2021, **42**, 101949.

23 J. Zhang, L. Han, H. Wu, Y. Zhong, P. Shangguan, Y. Liu, M. He, H. Sun, C. Song, X. Wang, Y. Liu, J. Wang, L. Zheng, B. Shi and B. Z. Tang, A Brain–Targeting NIR–II ferroptosis System: Effective visualization and oncotherapy for orthotopic glioblastoma, *Adv. Sci.*, 2023, **10**, e2206333.

24 K. Xiao, N. Zhang, F. Li, D. Hou, X. Zhai, W. Xu, G. Wang, H. Wang and L. Zhao, Pro-oxidant response and accelerated ferroptosis caused by synergetic Au(ı) release in hypercarbon-centered gold(ı) cluster prodrugs, *Nat. Commun.*, 2022, **13**, 4669.

25 P. Arnaut, N. B. Pozsoni, D. Bondar, P. Lippmann, S. Boschuk, I. Semenyuta, S. Bhandary, K. Van Hecke, Y. Karpichev, E. Cavarzerani, V. Canzonieri, F. Rizzolio, T. Scattolin, G. C. Vougioukalakis, I. Ott, N. V. Tzouras and S. P. Nolan, A new generation of N-heterocyclic carbene (NHC) gold–selenolato complexes as potent anticancer agents: distinct synthetic routes and evaluation in 2D and 3D cancer models, *Chem. Sci.*, 2025, **16**, 17221–17231.

26 A. J. Arduengo, R. Krafczyk, R. Schmutzler, H. A. Craig, J. R. Goerlich, W. J. Marshall and M. Unverzagt, Imidazolylidenes, imidazolinylidenes and imidazolidines, *Tetrahedron*, 1999, **55**, 14523–14534.

27 D. V. Pasyukov, M. A. Shevchenko, A. V. Astakhov, M. E. Minyaev, Y. Zhang, V. M. Chernyshev and V. P. Ananikov, New class of RSO2-NHC ligands and Pd/RSO2-NHC complexes with tailored electronic properties and high performance in catalytic C–C and C–N bonds formation, *Dalton Trans.*, 2023, **52**, 12067–12086.

28 G. Meng, L. Kakalis, S. P. Nolan and M. Szostak, A simple ^{1}H NMR method for determining the σ-donor properties of N-heterocyclic carbenes, *Tetrahedron Lett.*, 2018, **60**, 378–381.

29 S. P. Nolan, The development and catalytic uses of N-Heterocyclic carbene gold complexes, *Acc. Chem. Res.*, 2010, **44**, 91–100.

30 C. M. Friend and A. S. K. Hashmi, Gold catalysis, *Acc. Chem. Res.*, 2014, **47**, 729–730.

31 A. Collado, A. Gómez-Suárez, A. R. Martin, A. M. Z. Slawin and S. P. Nolan, Straightforward synthesis of [Au(NHC)X] (NHC = N-heterocyclic carbene, X = Cl, Br, I) complexes, *Chem. Commun.*, 2013, **49**, 5541.

32 A. Simoens, T. Scattolin, T. Cauwenbergh, G. Pisanò, C. S. J. Cazin, C. V. Stevens and S. P. Nolan, Continuous flow synthesis of Metal–NHC complexes, *Chem. – Eur. J.*, 2021, **27**, 5653–5657.

33 T. Scattolin, N. V. Tzouras, L. Falivene, L. Cavallo and S. P. Nolan, Using sodium acetate for the synthesis of [Au(NHC)X] complexes, *Dalton Trans.*, 2020, **49**, 9694–9700.

34 (*a*) R. Saito, A. Prato, A. Rubbi, L. Orian, T. Scattolin and S. P. Nolan, Simple synthesis of [Au(NHC)X] complexes utilizing aqueous ammonia: revisiting the weak base route mechanism, *Dalton Trans.*, 2024, **54**, 59–64; (*b*) R. Saito, P. Arnaut, B. Maliszewski, L. Tripodi, I. Caligiuri, F. Rizzolio, T. Scattolin and S. P. Nolan, Facile and green synthesis of [Pd(NHC)(η3-R-allyl)Cl] complexes and their anticancer activity, *Dalton Trans.*, 2025, **54**, 11720–11724.

35 N. V. Tzouras, F. Nahra, L. Falivene, L. Cavallo, M. Saab, K. Van Hecke, A. Collado, C. J. Collett, A. D. Smith, C. S. J. Cazin and S. P. Nolan, A mechanistically and operationally simple route to Metal–N–Heterocyclic carbene (NHC) complexes, *Chem. – Eur. J.*, 2020, **26**, 4515–4519.

36 R. Gauthier, N. V. Tzouras, Z. Zhang, S. Bédard, M. Saab, L. Falivene, K. Van Hecke, L. Cavallo, S. P. Nolan and J. Paquin, Gold N–Heterocyclic carbene catalysts for the hydrofluorination of alkynes using hydrofluoric acid: reaction scope, mechanistic studies and the tracking of elusive intermediates, *Chem. – Eur. J.*, 2021, **28**, e202103886.

37 M. Pažický, A. Loos, M. J. Ferreira, D. Serra, N. Vinokurov, F. Rominger, C. Jäkel, A. S. K. Hashmi and M. Limbach, Synthesis, reactivity, and electrochemical studies of Gold(ı) and Gold(ııı) complexes supported by N-Heterocyclic carbenes and their application in catalysis, *Organometallics*, 2010, **29**, 4448–4458.

38 D. V. Partyka, M. Zeller, A. D. Hunter and T. G. Gray, Relativistic functional groups: aryl Carbon–Gold bond formation by selective transmetalation of boronic acids, *Angew. Chem., Int. Ed.*, 2006, **45**, 8188–8191.

39 S. Dupuy, L. E. Crawford, M. Bühl, A. M. Z. Slawin and S. P. Nolan, The role of metal hydroxide complexes in Late Transition Metal–Mediated Transmetalation Reaction: the case of Gold, *Adv. Synth. Catal.*, 2012, **354**, 2380–2386.

40 N. V. Tzouras, M. Saab, W. Janssens, T. Cauwenbergh, K. Van Hecke, F. Nahra and S. P. Nolan, Simple synthetic routes to N–Heterocyclic carbene Gold(ı)–Aryl complexes: expanded scope and reactivity, *Chem. – Eur. J.*, 2020, **26**, 5541–5551.

41 N. V. Tzouras, N. B. Pozsoni, G. Carì, R. Saito, T. a. C. A. Bayrakdar, S. Bhandary, K. Van Hecke, G. C. Vougioukalakis and S. P. Nolan, Synthesis of N–Heterocyclic carbene AU(I)–Aryl complexes through mild Base–Assisted transmetallation of arylboronic acids: scope and limitations, *Chem. – Eur. J.*, 2025, e03322.

42 T. Cauwenbergh, N. V. Tzouras, T. Scattolin, S. Bhandary, A. Simoens, K. Van Hecke, C. V. Stevens and S. P. Nolan, Continuous flow synthesis of [Au(NHC)(Aryl)] (NHC=N–Heterocyclic carbene) complexes, *Chem. – Eur. J.*, 2021, **27**, 13342–13345.

43 T. Scattolin, A. Simoens, C. V. Stevens and S. P. Nolan, Flow chemistry of main group and transition metal complexes, *Trends Chem.*, 2022, **4**, 584–607.

44 K. K. Pandey, Theoretical insights into the relative bonding of normal and abnormal N-heterocyclic carbenes in [PdCl2(NHCR)2] and [PdCl2(NHCR)(aNHCR)] (R = H, Ph, Mes), *Int. J. Quantum Chem.*, 2016, **116**(7), 537–546.

45 G. Tonon, M. Mauceri, E. Cavarzerani, R. Piccolo, C. Santo, N. Demitri, L. Orian, P. A. Nogara, J. B. T. Rocha, V. Canzonieri, F. Rizzolio, F. Visentin and T. Scattolin, Unveiling the promising anticancer activity of palladium (ıı)-aryl complexes bearing diphosphine ligands: a structure-activity relationship analysis, *Dalton Trans.*, 2024, **53**, 8463–8477.

46 A. Madabeni, T. Scattolin, E. Bortolamiol, F. Visentin and L. Orian, Reactivity of Palladium(ıı)-η3-Allyl Complexes with Chalcogenolates: A Density Functional Study of Their Antitumor Implications, *Organometallics*, 2024, **43**(9), 954–962.

47 T. Scattolin, I. Pessotto, E. Cavarzerani, V. Canzonieri, L. Orian, N. Demitri, C. Schmidt, A. Casini, E. Bortolamiol, F. Visentin, F. Rizzolio and S. P. Nolan, Indenyl and Allyl Palladate Complexes Bearing N-Heterocylic Carbene Ligands: an Easily Accessible Class of New Anticancer Drug Candidates, *Eur. J. Inorg. Chem.*, 2022, **16**, e202200103.

48 D. Zeppilli, A. Madabeni, P. A. Nogara, J. B. T. Rocha and L. Orian, Reactivity of Zinc Fingers in Oxidizing Environments: Insight from Molecular Models Through Activation Strain Analysis, *ChemPlusChem*, 2024, **89**, e202400252.

49 A. Madabeni, P. A. Nogara, M. Bortoli, J. B. T. Rocha and L. Orian, Effect of Methylmercury Binding on the Peroxide-Reducing Potential of Cysteine and Selenocysteine, *Inorg. Chem.*, 2021, **60**(7), 4646–4656.

50 M. S. Filho, T. Scattolin, P. Dao, N. V. Tzouras, R. Benhida, M. Saab, K. Van Hecke, P. Lippmann, A. R. Martin, I. Ott and S. P. Nolan, Straightforward synthetic route to gold(ı)-thiolato glycoconjugate complexes bearing NHC ligands (NHC = N-heterocyclic carbene) and their promising anticancer activity, *New J. Chem.*, 2021, **45**, 9995–10001.

51 G. Genchi, G. Lauria, A. Catalano, M. S. Sinicropi and A. Carocci, Biological activity of selenium and its impact on human health, *Int. J. Mol. Sci.*, 2023, **24**, 2633.

52 W. Eikens, C. Kienitz, P. G. Jones and C. Thöne, Gold complexes with selenium ligands. Part 7. Synthesis and crystal structures of oligonuclear gold(ı)-selenolate complexes, *J. Chem. Soc., Dalton Trans.*, 1994, 83–90.

53 O. Crespo, M. C. Gimeno, A. Laguna, M. Kulcsar and C. Silvestru, Gold Complexes with the Selenolate Ligand [2-(Me2NCH2)C6H4Se]−, *Inorg. Chem.*, 2009, **48**, 4134–4142.

54 S. Canales, O. Crespo, M. C. Gimeno, P. G. Jones and A. Laguna, Selenolate Gold Complexes with Aurophilic Au(I)−Au(I) and Au(I)−Au(III) Interactions, *Inorg. Chem.*, 2004, **43**, 7234–7238.

55 J. C. Dearden and G. M. Bresnen, The measurement of partition coefficients, *QSAR*, 1988, **7**, 133–144.

56 M. G. Brattain, A. E. Levine, S. Chakrabarty, L. C. Yeoman, J. K. V. Willson and B. Long, Heterogeneity of human colon carcinoma, *Cancer Metastasis Rev.*, 1984, **3**, 177–191.

57 N. Harbeck, F. Penault-Llorca, J. Cortes, M. Gnant, N. Houssami, P. Poortmans, K. Ruddy, J. Tsang and F. Cardoso, Breast cancer, *Nat. Rev. Dis. Primers*, 2019, **5**, 66.

58 A. Stathis and M. J. Moore, Advanced pancreatic carcinoma: current treatment and future challenges, *Nat. Rev. Clin. Oncol.*, 2010, **7**, 163–172.

59 W. Zhang, L.-M. Yang, Y. Zhao, M.-Y. Li, Y.-Q. Shi, Y. Lu, X.-S. Wang, S. He, F.-Y. Wang, K.-B. Huang and H. Liang, Stable cyclometalated Gold(III) complex engaging isoquinoline derivative and disulfur ligand elicits Necroptosis-Dependent immunogenic cell death, *J. Med. Chem.*, 2026, **69**, 4932–4944.

60 D. Bratosin, L. Mitrofan, C. Palii, J. Estaquier and J. Montreuil, Novel fluorescence assay using calcein–AM for the determination of human erythrocyte viability and aging, *Cytometry, Part A*, 2005, **66A**, 78–84.

61 W. A. Dengler, J. Schulte, D. P. Berger, R. Mertelsmann and H. H. Fiebig, Development of a propidium iodide fluorescence assay for proliferation and cytotoxicity assays, *Anti-Cancer Drugs*, 1995, **6**, 522–532.

62 A. Gomes, E. Fernandes and J. L. F. C. Lima, Fluorescence probes used for detection of reactive oxygen species, *J. Biochem. Biophys. Methods*, 2005, **65**, 45–80.

63 J. Karges, Reactive Oxygen Species Detection with Fluorescent Probes: Limitations and Recommendations beyond DCFH-DA, *J. Med. Chem.*, 2026, **69**, 1970–1981.

64 W. S. Yang and B. R. Stockwell, Ferroptosis: death by lipid peroxidation, *Trends Cell Biol.*, 2015, **26**, 165–176.

65 Y. Su, B. Liu, B. Wang, L. Chan, C. Xiong, L. Lu, X. Zhang, M. Zhan and W. He, Progress and Challenges in Tumor Ferroptosis Treatment Strategies: A Comprehensive review of metal complexes and nanomedicine, *Small*, 2024, **20**, e2310342.

66 N. Montesdeoca, L. Johannknecht, E. Efanova, J. Heinen-Weiler and J. Karges, Ferroptosis inducing CO(III) polypyridine sulfasalazine complex for therapeutically enhanced anticancer therapy, *Angew. Chem., Int. Ed.*, 2024, **63**, e202412585.

67 N. Montesdeoca, H. M. Tran, S. K. Hinojosa, H. Sielhorst, J. Heinen-Weiler and J. Karges, Hydroxyl Radical Photoredox Catalysis in Hypoxic Cancer Cells, *ChemRxiv*, preprint, 2025, DOI: **10.26434/chemrxiv-2025-gr5gf**.

68 A. M. Martinez, A. Kim and W. S. Yang, Detection of ferroptosis by BODIPYTM 581/591 C11, *Methods Mol. Biol.*, 2020, **2108**, 125–130.

69 Y. Sun, Y. Zheng, C. Wang and Y. Liu, Glutathione depletion induces ferroptosis, autophagy, and premature cell senescence in retinal pigment epithelial cells, *Cell Death Dis.*, 2018, **9**, 753.

70 B. S. Mandavilli and M. S. Janes, Detection of intracellular glutathione using ThiolTracker violet stain and fluorescence microscopy, *Curr. Protoc. Cytom.*, 2010, **53**, DOI: **10.1002/0471142956.cy0935s53**.

71 P. T. Lieu, M. Heiskala, P. A. Peterson and Y. Yang, The roles of iron in health and disease, *Mol. Asp. Med.*, 2001, **22**, 1–87.

72 H. Wang, W. Mao, Y. Zhang, W. Feng, B. Bai, B. Ji, J. Chen, B. Cheng and F. Yan, NOX1 triggers ferroptosis and ferritinophagy, contributes to Parkinson's disease, *Free Radicals Biol. Med.*, 2024, **222**, 331–343.

73 (*a*) CCDC 2518319: Experimental Crystal Structure Determination, 2026, DOI: **10.5517/ccdc.csd.cc2qjj3x**; (*b*) CCDC 2518320: Experimental Crystal Structure Determination, 2026, DOI: **10.5517/ccdc.csd.cc2qjj4y**; (*c*) CCDC 2518321: Experimental Crystal Structure Determination, 2026, DOI: **10.5517/ccdc.csd.cc2qjj5z**; (*d*) CCDC 2518322: Experimental Crystal Structure Determination, 2026, DOI: **10.5517/ccdc.csd.cc2qjj60**; (*e*) CCDC 2518323: Experimental Crystal Structure Determination, 2026, DOI: **10.5517/ccdc.csd.cc2qjj71**; (*f*) CCDC 2518324: Experimental Crystal Structure Determination, 2026, DOI: **10.5517/ccdc.csd.cc2qjj82**; (*g*) CCDC 2518325: Experimental Crystal Structure Determination, 2026, DOI: **10.5517/ccdc.csd.cc2qjj93**; (*h*) CCDC 2518326: Experimental Crystal Structure Determination, 2026, DOI: **10.5517/ccdc.csd.cc2qjjb4**; (*i*) CCDC 2518327: Experimental Crystal Structure Determination, 2026, DOI: **10.5517/ccdc.csd.cc2qjjc5**; (*j*) CCDC 2518328: Experimental Crystal Structure Determination, 2026, DOI: **10.5517/ccdc.csd.cc2qjjd6**; (*k*) CCDC 2518329: Experimental Crystal Structure Determination, 2026, DOI: **10.5517/ccdc.csd.cc2qjjf7**; (*l*) CCDC 2518330: Experimental Crystal Structure Determination, 2026, DOI: **10.5517/ccdc.csd.cc2qjjg8**.